NASA TN D-1299

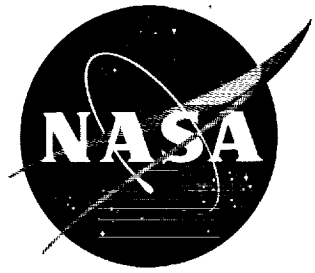

TECHNICAL NOTE

D-1299

FREE-FLIGHT MEASUREMENTS OF THE STATIC AND DYNAMIC STABILITY AND DRAG OF A 10° BLUNTED CONE AT MACH NUMBERS 3.5 AND 8.5

By Peter F. Intrieri

Ames Research Center
Moffett Field, Calif.

NATIONAL AERONAUTICS AND SPACE ADMINISTRATION

WASHINGTON May 1962

NATIONAL AERONAUTICS AND SPACE ADMINISTRATION

TECHNICAL NOTE D-1299

FREE-FLIGHT MEASUREMENTS OF THE STATIC AND DYNAMIC STABILITY AND DRAG OF A 10° BLUNTED CONE AT MACH NUMBERS 3.5 AND 8.5

By Peter F. Intrieri

SUMMARY

Tests were made of a short blunt-nosed 10° half-angle cone with and without a 50° half-angle conical afterbody in a pressurized ballistic range at nominal Mach numbers of 3.5 and 8.5 and nominal Reynolds numbers of 90,000 and 220,000, respectively. It was found that the models were statically stable about the center-of-gravity location tested but exhibited neutral dynamic stability for flight at constant altitude. The static stability was not affected by the 50° half-angle conical afterbody, but was nonlinear with angle of attack and varied with Mach number. The nonlinear variation of the pitching moment with angle of attack was accurately approximated by a cubic polynomial. The static stability was only qualitatively predicted by modified Newtonian theory. The drag characteristics were in good agreement with values calculated by use of modified Newtonian theory.

Calculations of the oscillatory behavior of the configurations flying an example entry trajectory through the Martian atmosphere indicated the configurations to be dynamically satisfactory. Pitching motions should converge to a small fraction of the amplitude at entry, provided the initial angle of attack and pitch rate are not large enough to cause tumbling.

INTRODUCTION

A coordinated study program has been undertaken at the Ames Research Center to provide information on aerodynamic problems associated with the design of probe vehicles for entry into planetary atmospheres. One of the problems is providing the required aerodynamic stability for orienting the vehicle properly during the early phase of entry prior to the point of maximum heating. Achieving the required orientation through the use of aerodynamic stability alone would be desirable and would result in a completely passive system. Another problem concerns the oscillatory behavior of the vehicle as it descends through a planetary atmosphere.

It has been shown in references 1 and 2 that divergent oscillations can begin near the altitude at which dynamic pressure is a maximum. Whether divergent oscillations will or will not begin at this altitude depends on the aerodynamic damping of the vehicle.

As part of the coordinated program, this investigation was conducted to determine the static and dynamic stability and drag at Mach numbers of 3.5 and 8.5 of a configuration believed representative of suitable probe vehicles. The configuration selected was a blunt-nosed 10° half-angle cone with a flat base which is known to satisfy many of the requirements of an entry vehicle. However, previous tests have shown that flat-based bodies of revolution are generally statically stable about two trim attitudes, one nose forward and one base forward. Thus this type of vehicle could, without proper initial orientation, be trimmed in the base-forward attitude, in which case it would not be properly protected against aerodynamic heating. Therefore the base geometry was modified to provide a unique nose-forward stable attitude of the vehicle. The required orientation stability was achieved by a rearward-pointing conical afterbody added to the base. The conical afterbody selected was the shortest one which would adequately provide this stability, a 50° half-angle cone. Exploratory investigations were also made of the model without afterbody to determine the effect of the afterbody on the aerodynamic characteristics.

A 6 0 4

Results of another phase of the coordinated program are presented in reference 3. In that investigation the stability characteristics of the models with and without afterbody were obtained for Mach numbers from 0.60 to 2.2. The present investigation was conducted in the Ames Pressurized Ballistic Range at nominal Mach numbers of 3.5 and 8.5 and Reynolds numbers of 90,000 and 220,000, respectively, based on free-stream conditions and model diameter. The models were tested in air; hence, the results obtained are applicable for entry of these vehicles into the earth's atmosphere. However, available information (see, e.g., ref. 4) indicates that the Martian atmosphere is composed predominantly of nitrogen which has thermodynamic properties very similar to those of air. Therefore, the results obtained in the present investigation should be applicable for entry of these vehicles into the Martian atmosphere.

SYMBOLS

A	reference area, maximum body cross-sectional area, sq ft
C	arbitrary constant in equation (8)
C_D	drag coefficient, $\frac{\text{total drag}}{q_\infty A}$

C_{L_α}	lift-curve slope, per radian
C_m	pitching-moment coefficient, $\frac{\text{pitching moment}}{q_\infty Ad}$, dimensionless
C_{m_α}	pitching-moment-curve slope, per radian
$C_{m_q} + C_{m_{\dot\alpha}}$	damping-in-pitch derivative, $\frac{\partial C_m}{\partial(qd/V)} + \frac{\partial C_m}{\partial(\dot\alpha d/V)}$, per radian
C_{N_α}	normal-force-curve slope, per radian
d	reference diameter, maximum body diameter, ft
g	acceleration due to gravity, ft/sec^2
H	geopotential altitude, ft
I_y	transverse moment of inertia, $m\sigma^2$, slug-ft^2
k	constant in equation (1), dimensionless
K	dynamic stability parameter for variable density (eq. (9)), dimensionless
$K_{1,2,3}$	constants in equation (3), deg
m	mass of model, slugs
M	Mach number, dimensionless
M_1	defined by equation (A2), ft^{-2}
$M_{2,3}$	cubic restoring moment coefficients, defined by equation (A1), ft^{-2}
p	roll parameter, $\frac{\text{roll rate}}{\text{velocity}}$, radians/ft
q	angular pitching velocity, radians/sec
q_∞	free-stream dynamic pressure, lb/sq ft
R	universal gas constant, ft^2/sec^2 $^\circ$R
Re	Reynolds number based on free-stream air properties and maximum diameter, dimensionless
T	temperature, $^\circ$R

u	horizontal component of flight velocity, ft/sec
V	velocity along flight path, ft/sec
x_{cg}	axial distance from model nose to center-of-gravity position, ft
X,Y,Z	earth-fixed axes; also displacements along these axes, ft
α	angle of attack in earth-fixed axes (angle between model axis and resultant wind direction projected onto the vertical XZ plane), deg or radians
α_r	resultant angle of attack, $\sqrt{\alpha^2 + \beta^2}$, deg or radians
α_{rms}	root-mean-square resultant angle of attack, $\sqrt{\frac{\int_0^x \alpha_r^2}{x} dx}$, deg
β	angle of sideslip in earth-fixed axes (angle between model axis and resultant wind direction projected onto the horizontal XY plane), deg
γ	flight-path angle (referenced to the local horizontal), deg
$\eta_{1,2}$	damping exponents in equation (3), ft^{-1}
θ,ψ	attitude coordinates of the model relative to earth-fixed axes, deg
λ	wave length of pitching oscillation, ft/cycle
ξ	dynamic stability parameter for constant altitude (eq. (7)), dimensionless
ρ	atmospheric density, slugs/cu ft
σ	transverse radius of gyration, ft
$\omega_{1,2}$	ratio of rotation of complex vectors which generate the model pitching motion (eq. (3)), radians/ft
$(\dot{})$	first derivative with respect to time

Subscripts

cg	center of gravity
i	initial condition

max	maximum
min	minimum
o	condition at surface of planet
∞	free-stream conditions

DESCRIPTION OF TESTS

Models and Sabots

Sketches of the models showing pertinent nominal dimensions are shown in figure 1. The aftersection of each model was machined from 7076-T6 aluminum; the front sections of the models with and without afterbodies were machined from phosphor bronze and titanium, respectively, to obtain the same center-of-gravity location, 0.48 d from the nose. The position of the center of gravity for the models was measured accurate to within 0.001 inch. The small screw on the base of the flat-based model was used to secure the model to the sabot. The point on the base of the screw on this model and the apex of the 50° half-angle cone on the other model served as reference points for reading the position of the models in the shadowgraph pictures. The dimensions of the models for each configuration deviated only slightly from those shown in figure 1. Some of the measured physical characteristics of each model are listed in table I.

Photographs of the models with their respective sabots are presented in figure 2. The sabots were made of Lexan plastic and were split in two pieces, as shown. A hole drilled through the sabot allowed powder gases inside the sabot to separate the sabot halves from the model upon emerging from the gun muzzle. The model with afterbody was held in correct alinement in the sabot by gluing the afterbody in the conical section of the sabot.

Test Technique and Test Conditions

The models were tested in free flight by launching them from guns. A caliber 50 powder gas gun was used to obtain a nominal model velocity of 4,000 feet per second, and a caliber 50 shock-heated helium gun to obtain a nominal model velocity of 10,000 feet per second, corresponding to nominal Mach numbers of 3.5 and 8.5, respectively. The test environment was air at rest in the test section of the Ames Pressurized Ballistic Range. To obtain adequate definition of the motions of the models through

the test section with the given spacing of shadowgraph stations in the range, the frequency of oscillation of the model was reduced by conducting the tests at reduced static pressure. The test-section static pressure was adjusted to 1.5 psia, which gave the desired wave length of oscillation and corresponds to the Reynolds numbers shown in table I. (Table I lists the average values of Mach number and Reynolds number for each flight.)

The trajectory of the model through the test section was recorded over a 203-foot trajectory in 24 shadowgraph stations located at various intervals. Side and plan views of the model are recorded in each shadowgraph along with reference wires from which X, Y, Z, θ, and ψ coordinates could be read - the linear coordinates within 0.005 inch, and angles within 0.25°. The orientation angles θ and ψ were read relative to earth-fixed axes. Corrections were made for the angle between the resultant wind direction and earth-fixed axes to give values of α and β. Time of model flight between stations was recorded with a precision chronograph to within 5/8 microsecond. Typical shadowgraph pictures of the models in flight are presented in figure 3.

A 6 0 4

REDUCTION OF DATA

Drag

The determination of drag coefficient from the time-distance data was based on the procedure described in reference 5, in which a constant drag coefficient is assumed. A procedure applicable to cases where the drag coefficient varies with angle of attack is presented in reference 6. It is shown in this reference that if the drag coefficient varies with the square of the local resultant angle of attack, according to the relation

$$C_D = C_{D_o} + k\alpha_r^2 \tag{1}$$

the drag coefficient obtained by the method of reference 5, under certain additional constraints, is the drag coefficient that would be obtained at a resultant angle of attack equal to the root-mean-square resultant angle of attack, α_{rms}, defined as

$$\alpha_{rms} = \left[\frac{\int_o^x (\alpha^2 + \beta^2)dx}{x}\right]^{1/2} \tag{2}$$

Stability Derivatives

Stability derivatives were obtained from analysis of the pitching and yawing motions of the models by fitting the following equation to the measurements of α and β of each flight.

$$\beta + i\alpha = K_1 e^{(\eta_1 + i\omega_1)x} + K_2 e^{(\eta_2 - i\omega_2)x} + K_3 e^{ipx} \tag{3}$$

Equation (3) is the solution of the linear differential equation of motion, as given in reference 7, and includes effects of model spin and trim angle on the motion. Some of the basic assumptions used in the development of this equation are: axially symmetric configuration, linear variations of force and moment with angle of attack, small angular displacements, and small angles of trim. Equation (3) programmed for machine computation for the investigation reported in reference 8 was used to select optimum values of the constants by an iterative process of differential corrections.

The static stability derivative, C_{m_α}, was computed from the wave length of oscillation by means of the following relation applicable to linear moment curves

$$-C_{m_\alpha} = \frac{8\pi^2 I_y}{\lambda^2 \rho A d} \tag{4}$$

where

$$\lambda = \frac{2\pi}{\sqrt{\omega_1 \omega_2}} \tag{5}$$

The dynamic stability parameter, ξ, was determined from the constants η_1 and η_2 by means of the relation

$$\eta_1 + \eta_2 = \frac{\rho A}{2m} \xi \tag{6}$$

where

$$\xi = C_D - C_{I_\alpha} + (C_{m_q} + C_{m_{\dot{\alpha}}})(d/\sigma)^2 \tag{7}$$

It has been shown in references 8 and 9 that ξ, in the form shown in equation (7), is a convenient parameter for describing the dynamic

stability of a vehicle in free flight at constant altitude. The values of ξ, presented in this report, were calculated with the assumption of a linear system over the angle-of-attack range covered by any one flight. Each value of ξ, therefore, is the dynamic stability parameter of an equivalent linear system whose amplitude of oscillation would grow or diminish in the same way as that experienced by the model.

Illustrations of the types of motions encountered in the present tests, as viewed in the α - β plane, are shown in figure 4. Since the models are aerodynamically symmetric, the angular displacement of the model, at any instant, can be represented also by the resultant angle of attack, α_r, whose orthogonal components are the angles α and β. It can be seen from figure 4 that, in general, the data show precessing elliptical motions, and that the angle range through which the models oscillate differs for each flight. The curves shown in figure 4 were obtained by fitting equation (3) to the experimental data. The fitted curves agreed with the measured angles within the measuring accuracy.

A 6 0 4

RESULTS AND DISCUSSION

A total of 15 flights were made for analysis of static stability, dynamic stability, and drag. Ten flights were made of models with afterbody (five each at Mach numbers 3.5 and 8.5), and five flights of models without afterbody (three at Mach number 3.5 and two at Mach number 8.5). Experimental values of C_{m_α}, ξ, $C_{m_q} + C_{m_{\dot{\alpha}}}$, and C_D are summarized in table I. Theoretical estimates of C_D, C_m, and C_{m_α} were made, using the equations developed in reference 10, based on Newtonian theory. The theory was modified by use of the stagnation-pressure coefficient behind a normal shock wave.

Drag

The measured values of drag coefficient plotted as a function of the root-mean-square resultant angle of attack in figure 5 show that the drag increases slightly (approximately 14 percent) as the angle of attack is increased from 0° to 28°. These data also show no measurable difference in the drag of the two configurations in this angle-of-attack range, but indicate a slight decrease (approximately 5 percent) as the Mach number is increased from 3.5 to 8.5. Values of C_D estimated by modified Newtonian theory, also included in this figure, show close agreement with the measured values but indicate an opposite trend with Mach number.

Static Stability

The experimental values of the equivalent linear pitching-moment-curve slope, C_{m_α}, are presented in figure 6, for both afterbody configurations, as a function of the maximum resultant angle of attack, $\alpha_{r_{max}}$. The data have been corrected for the small variations in center-of-gravity location shown in table I to a common center-of-gravity position, using the value of C_{N_α} at zero angle of attack estimated by modified Newtonian theory.

The data, presented in figure 6, show that although both configurations are statically stable throughout the angle-of-attack range investigated for Mach numbers 3.5 and 8.5, the stability decreases with increasing Mach number and increases with increasing angle of attack at each Mach number. The data also show no measurable difference in the stability of the two configurations, which indicates that the afterbody contributes little to the static stability in the angle-of-attack range covered here. The variation of C_{m_α} with angle of attack indicates the variation of the pitching moment with angle of attack is not linear for either configuration.

A method which permits analysis of the observed pitching and yawing motions of a symmetrical body having a nonlinear pitching moment to obtain local values of C_m and C_{m_α} is developed in reference 11 under the assumption that the nonlinear moment curve can be described by a linear term plus a cubic term. (The local value of C_m is that value which would be observed in a wind tunnel with the model held at a constant angle of attack.) Application of this method to the data of this report is discussed in the appendix. The local values of C_m and C_{m_α} computed by this procedure are presented in figures 7, 8, and 9. Comparison of these values of C_m, for Mach number 3.5, with unpublished wind-tunnel values for the same configuration at about the same Mach number in figure 7, shows that the data are in excellent agreement throughout the angle-of-attack range investigated. This agreement offers experimental evidence of the ability of the method developed in reference 11 to determine accurately from free-flight tests the local values of C_m and C_{m_α} for a symmetrical configuration with a nonlinear pitching moment. It should be pointed out that although the data compared in figure 7 were obtained at different Reynolds numbers, the results suggest no effect of Reynolds number on the stability of the present models in the range covered.

Comparison of the present experimental data at the two test Mach numbers, with modified Newtonian theory in figure 8, shows that the stability of the configurations at the lower angles of attack is reduced as the Mach number is increased from 3.5 to 8.5. Unpublished data for a model, similar to those used in the present test, fired in the Ames Supersonic Free-Flight Wind Tunnel at a Mach number of 15 are included in figures 8 and 9. At a Mach number of 15, the initial stability is the same as at Mach number 8.5. Furthermore, as the angle of attack is increased,

the stability is seen to increase more rapidly with increasing Mach number, so that at an angle of attack of about 40°, the configurations exhibit the highest level of stability at the highest Mach number. This increased nonlinearity of the pitching moment with angle of attack for increasing Mach number is more evident in figure 9, which shows the value of C_{m_α} at zero angle of attack to be about 75 percent greater for Mach number 3.5 than the value for Mach numbers 8.5 and 15; whereas, at an angle of attack of 33°, the value of C_{m_α} for Mach number 3.5 is about 40 percent less than the value for Mach number 15 and about 22 percent less than the value for Mach number 8.5.

Values of C_m and C_{m_α} estimated by modified Newtonian theory presented in figures 8 and 9 indicate the theory to be useful only for predicting qualitative trends and not for making quantitative estimates of the stability of these configurations.

Although experimental measurement of the static stability of the model with afterbody at angles of attack near 180° (backward orientation) was beyond the scope of the present investigation, one exploratory flight was made with the model launched backwards to determine whether it would remain flying backwards or, as expected from calculations, would begin righting itself to a nose-forward attitude. The model was launched at an angle of attack near 180° at a nominal velocity of 10,000 feet per second (M = 8.5) at the same conditions mentioned previously for the other flights. Examination of the photographic records of this flight showed that the model tumbled (in the vertical plane) throughout the 203-foot length of the test section.[1] Tumbling rates measured from the angular orientation-distance history of this flight at stations where the model was traversing 180° and 0° angle of attack indicated that the model emerged from the gun with an initial tumbling rate of 4° per foot and achieved a tumbling rate of 13.3° per foot at zero angle of attack. (The initial tumbling rate of 4° per foot resulted from the model-sabot separation process.) This observed initial tumbling rate and the pitching moments given by modified Newtonian theory were used to calculate the tumbling rate that would be expected at zero angle of attack. (It should be noted that according to modified Newtonian theory the model is stable only in the nose-forward attitude.) The calculated tumbling rate at zero angle of attack was 13.6° per foot, which is in excellent agreement with the measured value. Although the calculation is not sufficiently precise to discard the possibility of a small stable region occurring near 180° angle of attack, the excellent agreement between theory and experiment does suggest that this possibility is unlikely.

---

[1]Continued tumbling would be expected for [illegible]t at constant dynamic pressure as was the case here. However [illegible]ynamic pressure were to increase with time as it does for enti[illegible]o an atmosphere, the tumbling motion would be damped.

Dynamic Stability

The results of the dynamic stability measurements are presented in figure 10, where values of the dynamic stability parameter, ξ, are plotted as a function of the maximum resultant angle of attack, $\alpha_{r_{max}}$. Positive values of ξ represent a divergent model motion (dynamic instability), and negative values represent a convergent model motion (dynamic stability). Values of $\xi = 0$ represent a model motion that would neither diverge nor converge but would remain at a constant amplitude of oscillation (dynamically neutral). These data, presented in figure 10, show that for flights of both configurations, where the peak amplitude of oscillation is at least 7°, the measured values of ξ are very close to zero and indicate that the afterbody has little effect on the dynamic stability in this angle-of-attack range. The largest value of ξ is 0.65 and is equivalent to a divergence of less than 1 percent per cycle. As can be seen from figure 10, a value of $\xi = -3.25$ was measured from a flight of a model without afterbody with a peak amplitude of oscillation less than 3°. This value of ξ is approximately equivalent to a convergence of about 5 percent per cycle. To determine the largest reasonable variation in the experimental value of ξ for this flight, a probable error or 0.25° in the angle-of-attack measurements, determined statistically from many readings by several observers, was introduced to the input data of this flight. These errors oriented in the worst possible arrangement resulted in a change in the value of ξ of about 0.5. Therefore, it is indicated that the model without afterbody is dynamically stable in flight at constant altitude for amplitudes of oscillation near 3°. The effect of afterbody on the dynamic stability in this low-angle-of-attack range could not be determined since the minimum peak amplitude of oscillation obtained for models with afterbody was about 7°.

Values of the damping-in-pitch derivative, $C_{m_q} + C_{m_{\dot{\alpha}}}$, were calculated by means of equation (7) using the values of ξ (fig. 10) and C_D (fig. 5) measured from the present tests with values of C_{L_α} obtained from unpublished wind-tunnel measurements, and are presented in figure 11 as a function of $\alpha_{r_{max}}$. The damping-in-pitch derivative, $C_{m_q} + C_{m_{\dot{\alpha}}}$, is a measure of the dynamic stability of a model at constant flight velocity when the model is not free to plunge, for example, in wind-tunnel tests. These data show about the same trends, as those observed for values of ξ in figure 10, namely, small dynamic stability for the models without afterbody at $\alpha_{r_{max}}$ near 3°, and neutral or slight dynamic stability for both configurations at the higher angles of attack. It is interesting to note that whereas most of the values of ξ for $\alpha_{r_{max}}$ above 7° were slightly positive (see fig. 10), the corresponding values of $C_{m_q} + C_{m_{\dot{\alpha}}}$ for these same flights are seen to be slightly negative. Thus, the combination of C_D and C_{L_α} overshadow the stabilizing damping-in-pitch derivative to produce a divergent motion in these flights at constant altitude.

Application of the Present Results to a Full-Scale Vehicle Entering the Martian Atmosphere

To determine the significance of the present results when applied to a full-scale vehicle entering a planetary atmosphere, calculations were made of the oscillatory behavior of the present configurations flying an example entry trajectory through a model of the Martian atmosphere. To perform the calculations it was necessary to have available an example entry trajectory. This trajectory is required because studies of the oscillatory behavior of missiles entering the atmosphere on ballistic trajectories (ref. 1) have revealed that the rapid increase in atmospheric density experienced by such vehicles is a controlling factor governing the variations in magnitude of their oscillations. The following assumed initial conditions were used to compute the entry trajectory for this example:

$$V_i = 21{,}000 \text{ ft/sec}$$

$$\gamma_i = 40^\circ$$

$$H_i = 800{,}000 \text{ ft}$$

$$\frac{m}{C_D A} = 1.24 \text{ slugs/ft}$$

In addition, the well-known assumption that the atmospheric density varies exponentially with altitude was applied:

$$\rho = \rho_o e^{\frac{-g_o H}{RT}}$$

Available information (see, e.g., ref. 4) shows that approximate mean values of these parameters, for Mars, are

$$\rho_o = 0.000409 \text{ slug/ft}^3$$

$$T = 316^\circ \text{ R}$$

$$g_o = 13.16 \text{ ft/sec}^2$$

$$R = 1716 \text{ ft}^2/\text{sec}^2 \, {}^\circ\text{R}$$

These conditions define the entry trajectory considered.

An analysis which describes the oscillatory motions developed by vehicles as they descend through an atmosphere is presented in reference 2. In this reference it is shown that for constant aerodynamic coefficients the envelope of these oscillations has the simple form

$$\alpha_{max} = \frac{Cu^{-K/2}}{q_\infty^{1/4}} \tag{8}$$

(In the analysis the vehicle is assumed to be initially oriented nose forward with zero initial pitch rate.) Although the experimental data show the pitching moment to be nonlinear with angle of attack, the dynamic-stability results are seen to be linear with angle of attack. It follows that the use of equation (8) to study the oscillatory behavior of the present configurations will not be precisely valid, but it should be indicative of the dynamic behavior to be expected. It has also been shown in reference 2 that the dynamic stability parameter K, in the form

$$K = 1/C_D \left[-C_{L_\alpha} + (C_{m_q} + C_{m_{\dot{\alpha}}})(d/\sigma)^2 \right] \tag{9}$$

is a convenient parameter for describing the dynamic stability of a vehicle descending through a planetary atmosphere. It can be seen from a comparison of equations (7) and (9) that K can be expressed in terms of ξ and C_D as follows:

$$K = \frac{\xi}{C_D} - 1 \tag{10}$$

Values of K were computed using the measured values of ξ (see fig. 10) and C_D (fig. 5) and are presented in figure 12 as a function of $\alpha_{r_{max}}$. From these data it was considered that a value of K of -0.6 would be a reasonable mean value to use in equation (8). This value of K and the example entry trajectory were introduced in equation (8), expressed in ratio form, and values of the amplitude ratio $(\alpha/\alpha_i)_{max}$ were computed and are presented in figure 13 as a function of altitude. The results in this figure show that for K = -0.6 the amplitude ratio diminishes very rapidly; in fact, at 55,000 feet, the lowest altitude for which the calculations were performed, the amplitude of oscillation is less than 3 percent of the initial amplitude. Because of the scatter in the values of K (see fig. 12), it was decided to investigate the effect of small changes in K on the motion. For the case of K = 0, which from figure 12 appears to be the worst possible case, it can be seen in figure 13 that

the motion is divergent below the altitude for maximum dynamic pressure (approximately 130,000 feet), but the amplitude does not grow excessively. The amplitude of oscillation at 55,000 feet is still only about 8 percent of the initial amplitude. From these calculations, the oscillatory behavior of these configurations appears to be satisfactory for entry into the Martian atmosphere.

CONCLUSIONS

A 6 0 4

Ballistic-range tests conducted at Mach numbers 3.5 and 8.5 and Reynolds numbers of 90,000 and 220,000, respectively, of a blunt-nosed 10° half-angle cone with and without a 50° half-angle conical afterbody have led to the following conclusions.

1. The models were statically stable about the center-of-gravity location tested. The static stability was not affected by the 50° half-angle conical afterbody for angles of attack up to 32°, but was nonlinear with angle of attack and varied with Mach number.

2. The nonlinear variation of the pitching moment and pitching-moment-curve slope with angle of attack was accurately approximated by a cubic polynomial.

3. The models exhibited neutral dynamic stability for flight at constant altitude.

4. Modified Newtonian theory gave only qualitative estimates of the static stability and was not quantitatively accurate. The drag characteristics were in good agreement with the values calculated using modified Newtonian theory.

5. The oscillatory behavior of the present configurations appears to be dynamically satisfactory for entry into the Martian atmosphere. Pitching motions should converge to a small fraction of the amplitude at entry, provided the initial angle of attack and pitch rate are not large enough to cause tumbling.

Ames Research Center
National Aeronautics and Space Administration
Moffett Field, Calif., Jan. 9, 1962

APPENDIX A

APPLICATION OF NONLINEAR PITCHING-MOMENT ANALYSIS

A method which permits analysis of the pitching and yawing motions of a symmetrical body having a nonlinear pitching moment to obtain the local values of C_m and C_{m_α} is described in reference 11. The method assumes that the nonlinear pitching moment can be described by two terms, the first proportional to the resultant angle of attack, and the second proportional to the cube of the resultant angle of attack, of the form

$$M_1 = -M_2(\alpha_r) - 2M_3(\alpha_r)^3 \tag{A1}$$

where

$$M_1 = \frac{\rho A d}{2I_y} C_m \tag{A2}$$

A simple expression is then derived which relates the constants M_2 and M_3 in equation (A1) to the wave length of oscillation, λ, obtained from analysis of free-flight data using linear equations. For the present case, that is, a pitching moment that grows faster than a linear moment and for values of the ratio $(\alpha_{r_{min}}/\alpha_{r_{max}})^2$ from zero to one-half, the expression becomes (see ref. 11)

$$\left(\frac{2\pi}{\lambda}\right)^2 = M_2 + 1.44\, M_3 \left(\alpha_{r_{max}}{}^2 + \alpha_{r_{min}}{}^2\right) \tag{A3}$$

By use of this expression, values of the cubic restoring-moment coefficients, M_2 and M_3, can be obtained from the observed wave lengths and amplitudes of independent flights of the models at similar testing conditions. According to equation (A3), the applicability of the method to the data of this report rests on the approximate linear relationship of the observed frequency with the maximum and minimum amplitudes of the motion. Therefore, in order to determine the validity of the assumption of a cubic pitching-moment variation with angle of attack, the observed frequency $(2\pi/\lambda)^2$ was plotted as a function of the amplitudes of the motion $(\alpha_{r_{max}})^2 + (\alpha_{r_{min}})^2$ for each flight and is presented in

figure 14. It can be seen from this figure that the data fall very closely along straight lines for each Mach number, and therefore a cubic pitching-moment variation is an excellent approximation. It should be mentioned in relation to this figure that the measured wave lengths for the models without afterbody were adjusted so that the value of $\rho Ad/2I_y$ used in equation (A2) would be the same as the value used for the models with afterbody, which is 0.132 ft^{-2}. As can be seen from figure 14, these data fall on the same straight lines as do the data for the models with afterbody. Thus it is again shown that the afterbody contributes little to the stability over the angle-of-attack range investigated.

The data presented in figure 14 for each Mach number were fitted by the method of least squares, and the values of the coefficients M_2 and M_3 were found to be

Mach number	M_2	M_3
3.5	0.00935	0.00457
8.5	.00503	.00929

REFERENCES

1. Friedrich, Hans R., and Dore, Frank J.: The Dynamic Motion of a Missile Descending Through the Atmosphere. Jour. Aero. Sci., vol. 22, no. 9, Sept. 1955, pp. 628-632, 638.

2. Sommer, Simon C., and Tobak, Murray: Study of the Oscillatory Motion of Manned Vehicles Entering the Earth's Atmosphere. NASA MEMO 3-2-59A, 1959.

3. Wehrend, William R., Jr.: Wind-Tunnel Investigation of the Static and Dynamic Stability Characteristics of a 10° Semivertex Angle Blunted Cone. NASA TN D-1202, 1962.

4. Anon.: Studies of the Physical Properties of the Moon and Planets. Quarterly Technical Progress Report 4. Rand Corp., RM-2817-JPL, June 30, 1961.

5. Seiff, Alvin: A New Method for Computing Drag Coefficients From Ballistic Range Data. Jour. Aero. Sci., vol. 25, no. 2, Feb. 1958, pp. 133-134.

6. Seiff, Alvin, and Wilkins, Max E.: Experimental Investigation of a Hypersonic Glider Configuration at a Mach Number of 6 and at Full-Scale Reynolds Numbers. NASA TN D-341, 1961.

7. Nicolaides, John D.: On the Free Flight Motion of Missiles Having Slight Configurational Asymmetries. BRL Rep. 858, Aberdeen Proving Ground, Md., June 1953.

8. Short, Barbara J., and Sommer, Simon C.: Some Measurements of the Dynamic and Static Stability of Two Blunt-Nosed, Low-Fineness-Ratio Bodies of Revolution in Free-Flight at $M = 4$. NASA TM X-20, 1959.

9. Seiff, Alvin, Sommer, Simon C., and Canning, Thomas N.: Some Experiments at High Supersonic Speeds on the Aerodynamic and Boundary-Layer Transition Characteristics of High-Drag Bodies of Revolution. NASA RM A56I05, 1957.

10. Margolis, Kenneth: Theoretical Evaluation of the Pressures, Forces, and Moments at Hypersonic Speeds Acting on Arbitrary Bodies of Revolution Undergoing Separate and Combined Angle-of-Attack and Pitching Motions. NASA TN D-652, 1961.

11. Rasmussen, Maurice L.: Determination of Nonlinear Pitching-Moment Characteristics of Axially Symmetric Models From Free-Flight Data. NASA TN D-144, 1960.

TABLE I.- TEST CONDITIONS AND DATA

Flight	M	$Re \times 10^{-6}$	C_D	C_{m_α} (linear) $\frac{x_{cg}}{d} = 0.482$	ξ	$C_{m_q} + C_{m_{\dot{\alpha}}}$	K	$\alpha_{r_{max}}$, deg	$\alpha_{r_{min}}$, deg	α_{rms}, deg	$\frac{x_{cg}}{d}$	d, in.	$\left(\frac{d}{\sigma}\right)^2$	$I_y \times 10^8$, slug-ft^2
(a) Model with afterbody; nominal Mach number = 3.5														
310	3.56	0.094	0.795	-0.081	0.220	-0.032	-0.723	24.77	0.20	17.13	0.477	0.451	7.98	3.76
311	3.54	.093	.888	-.095	.110	-.057	-.876	40.95	.66	28.38	.476	.451	7.98	3.70
362	3.48	.092	.767	-.074	.177	-.034	-.769	19.81	.04	13.84	.483	.450	7.93	3.64
372	3.46	.091	.759	-.077	.234	-.025	-.692	18.92	.12	12.97	.485	.450	8.11	3.57
373	3.38	.085	.731	-.070	.334	-.010	-.543	7.72	.04	5.14	.485	.450	8.14	3.53
(b) Model with afterbody; nominal Mach number = 8.5														
355	8.52	.212	.799	-.077	-.220	-.097	-1.275	34.99	2.43	23.98	.481	.450	8.01	3.61
356	8.80	.221	.751	-.062	.684	.022	-.089	27.00	.35	18.54	.481	.450	8.00	3.61
357	8.74	.221	.763	-.058	.544	.003	-.287	21.52	11.47	16.99	.480	.450	7.98	3.59
369	8.99	.227	.753	-.066	.392	-.014	-.480	29.79	1.61	20.74	.485	.450	8.12	3.55
388	8.31	.207	.715	-.042	.328	-.005	-.542	12.32	.56	8.37	.486	.450	8.12	3.55
(c) Model without afterbody; nominal Mach number = 3.5														
302	3.43	.094	.734	-.067	-3.247	-.365	-5.42	2.85	.11	1.60	.473	.449	10.03	1.87
303	3.41	.091	.785	-.078	-.205	-.066	-1.261	22.01	.40	15.11	.472	.450	10.10	1.88
304	3.43	.090	.754	-.071	.379	-.005	-.498	11.27	.13	7.59	.473	.449	10.08	1.87
(d) Model without afterbody; nominal Mach number = 8.5														
359	8.69	.238	.778	-.067	-.084	-.061	-1.108	32.10	.23	22.01	.473	.449	10.09	1.85
390	8.77	.218	.758	-.064	.110	-.040	-.855	25.64	5.01	18.31	.473	.449	10.08	1.87

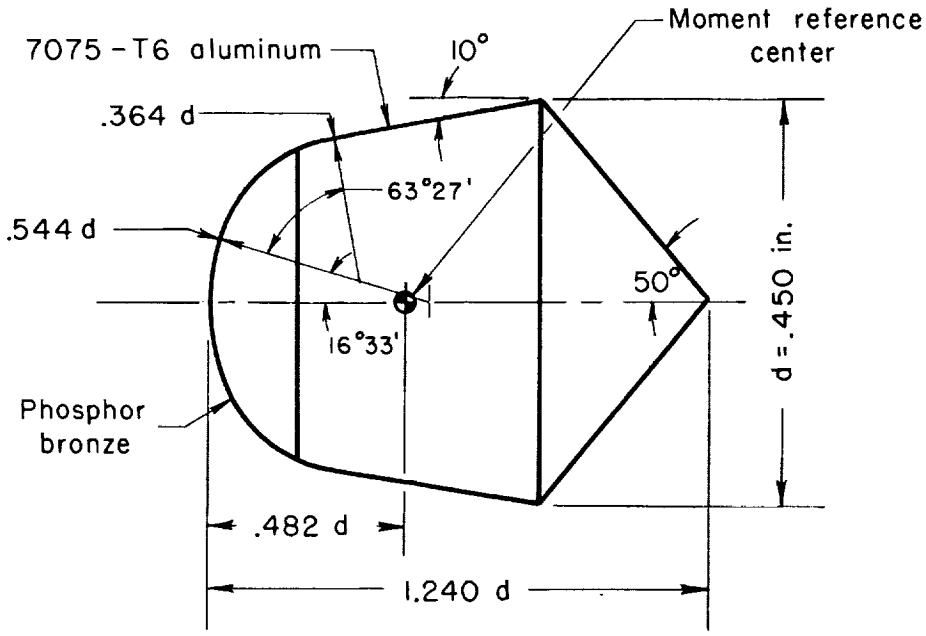

(a) Model with afterbody

Dimensions in inches except as noted

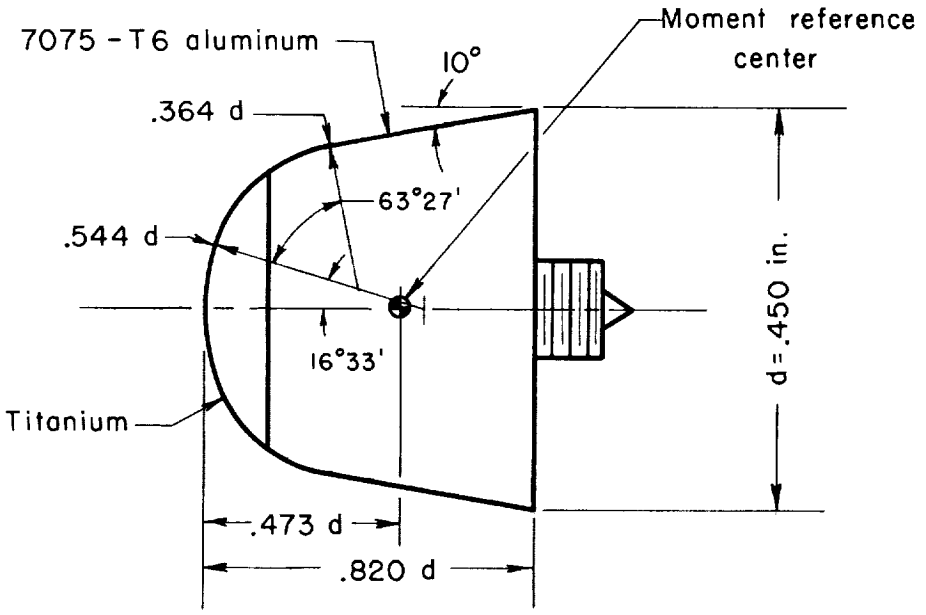

(b) Model without afterbody

Figure 1.- Sketches of models showing nominal dimensions.

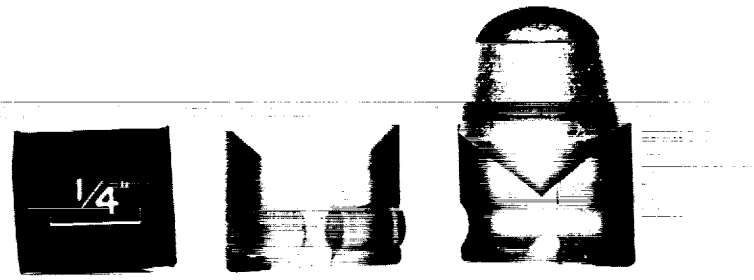

A-28479

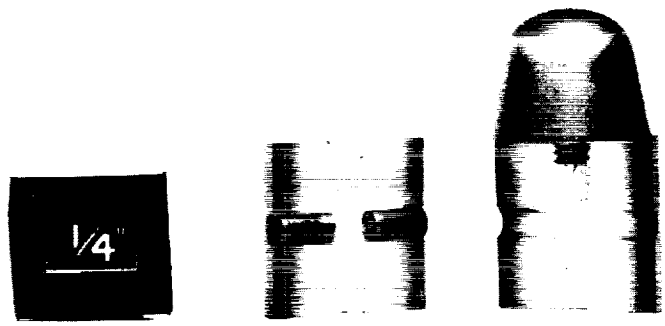

A-28480

Figure 2.- Photographs of models and sabots.

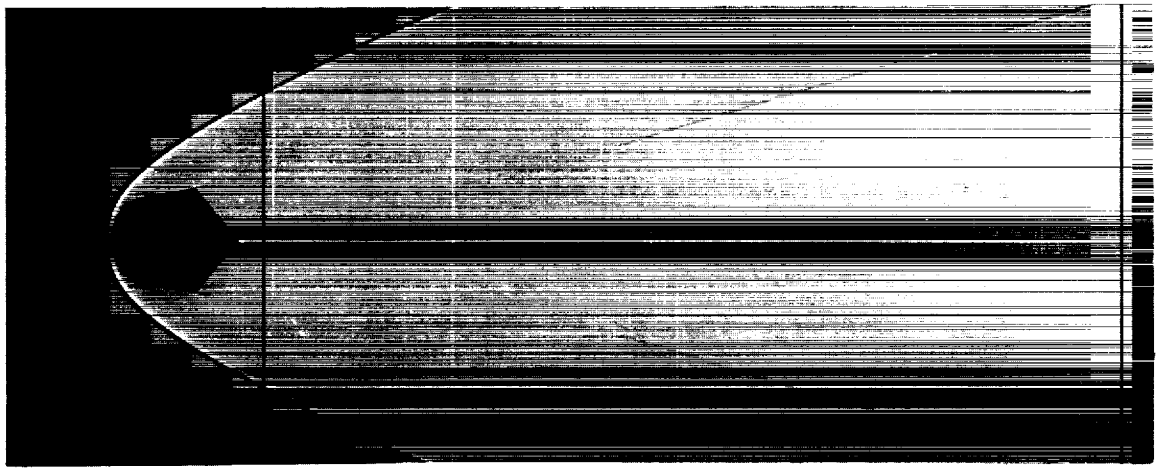

$\alpha = 0.11^{o}$

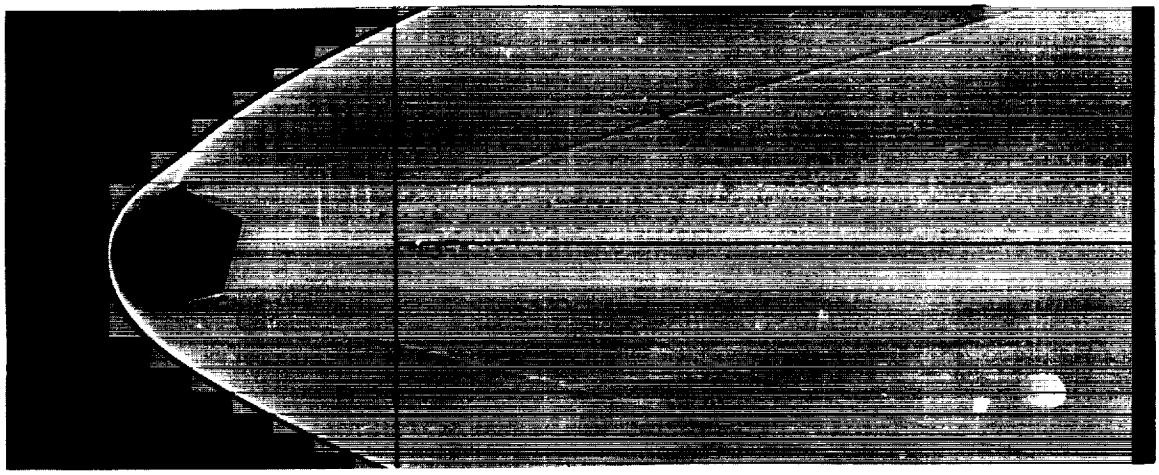

$\alpha = -22.92^{o}$

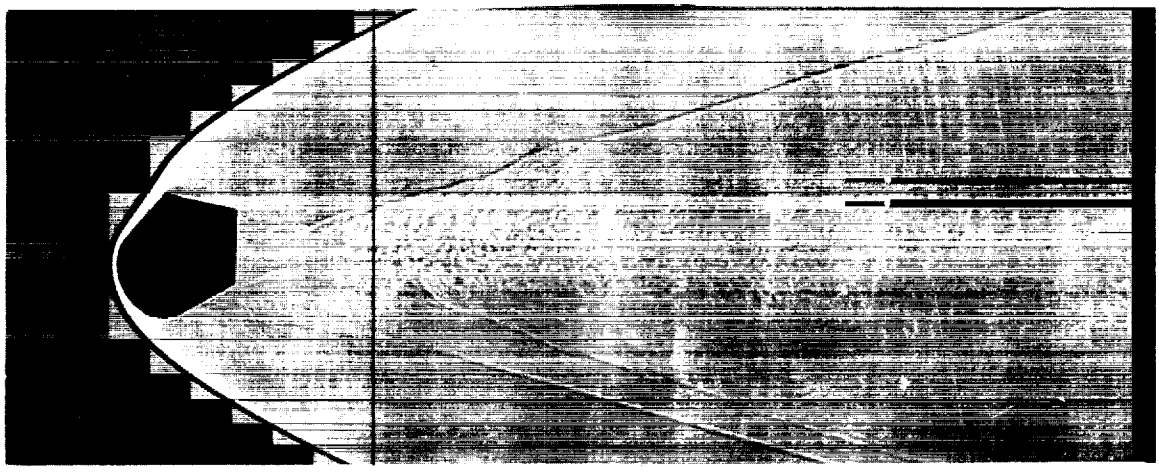

$\alpha = -39.32^{o}$

(a) M = 3.5, Re = 0.1×10^{6}

Figure 3.- Typical shadowgraphs of models in flight.

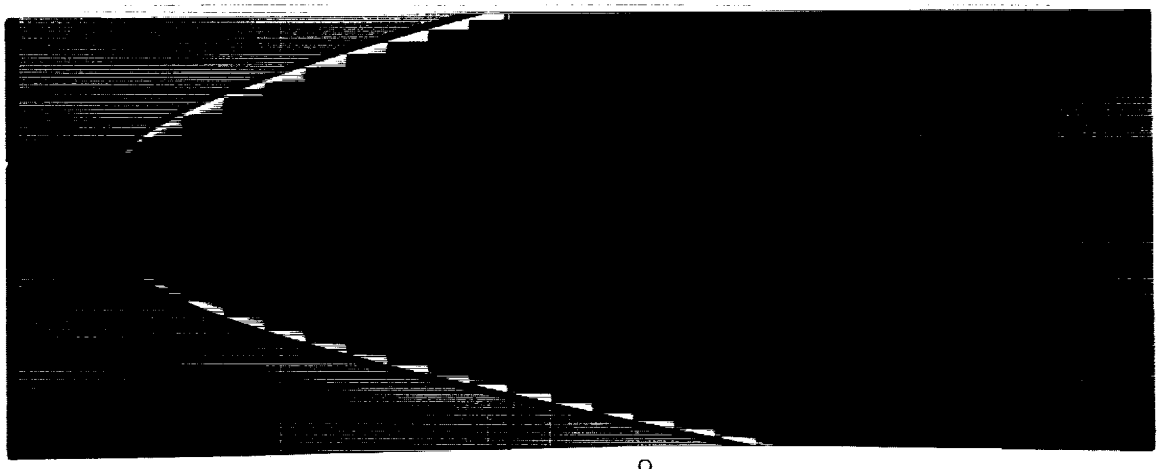

$\alpha = 0.39^{\circ}$

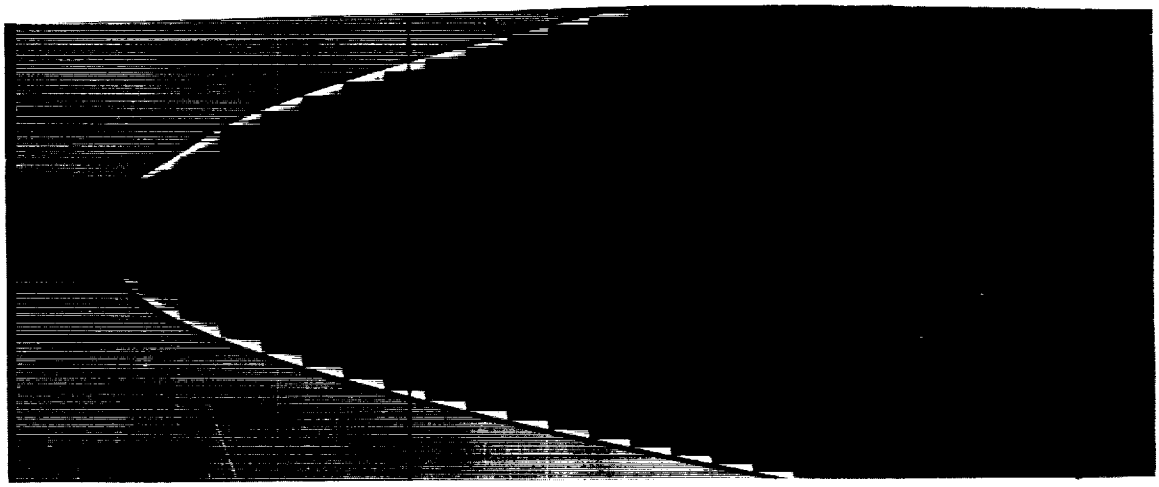

$\alpha = -21.67^{\circ}$

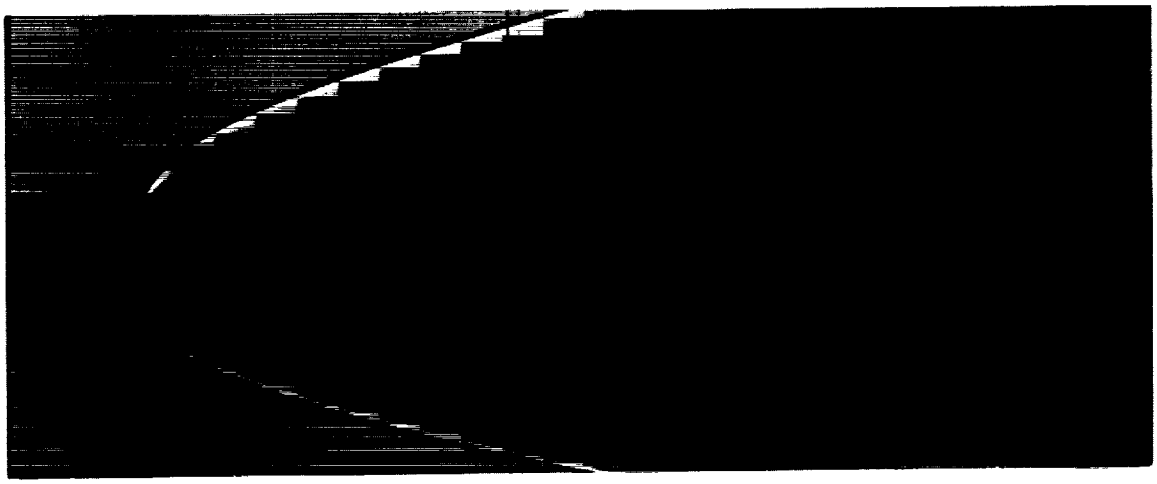

$\alpha = -34.42^{\circ}$

(b) M = 8.5, Re = 0.2×10^{6}

Figure 3.- Continued.

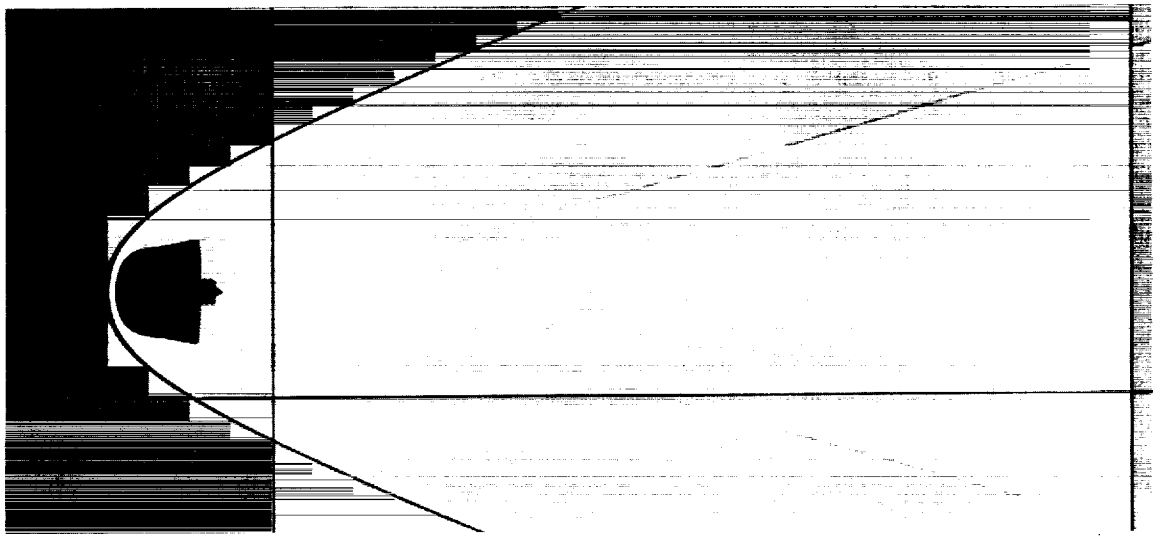

$\alpha = 0.47^{\circ}$

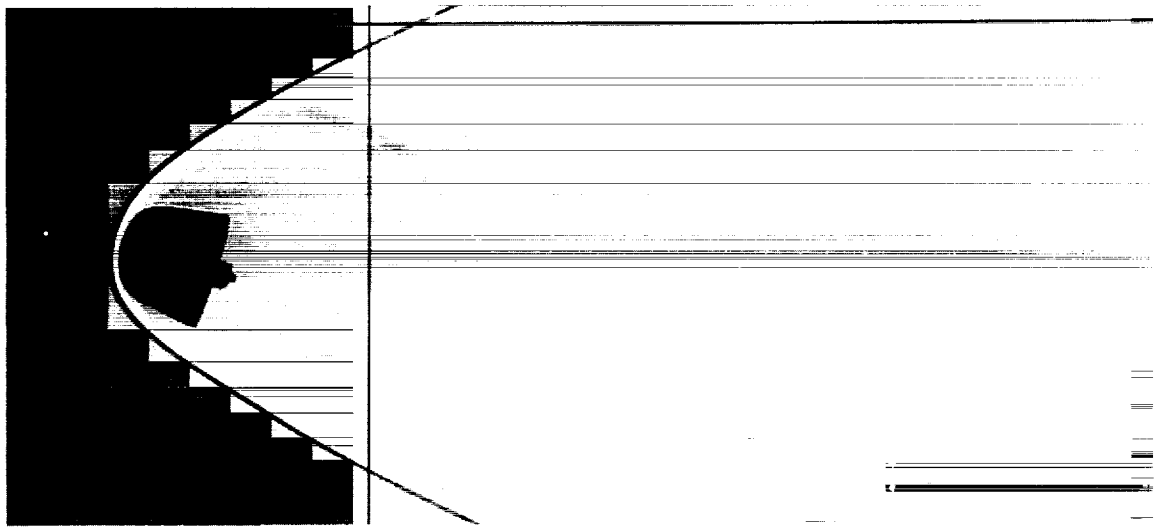

$\alpha = 16.95^{\circ}$

(c) $M = 3.5$, $Re = 0.1 \times 10^{6}$

Figure 3.- Continued.

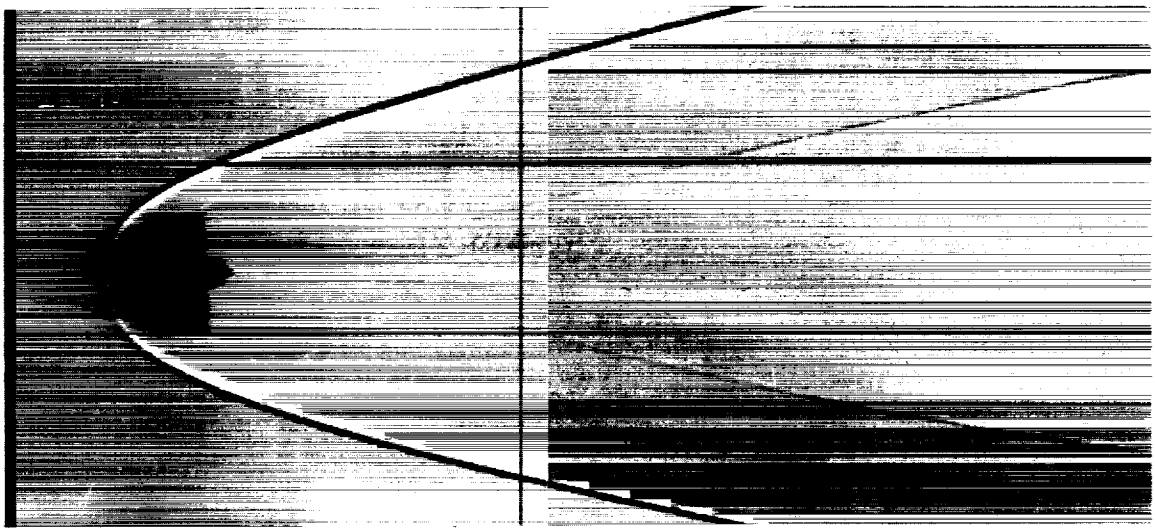

$\alpha = -3.34$

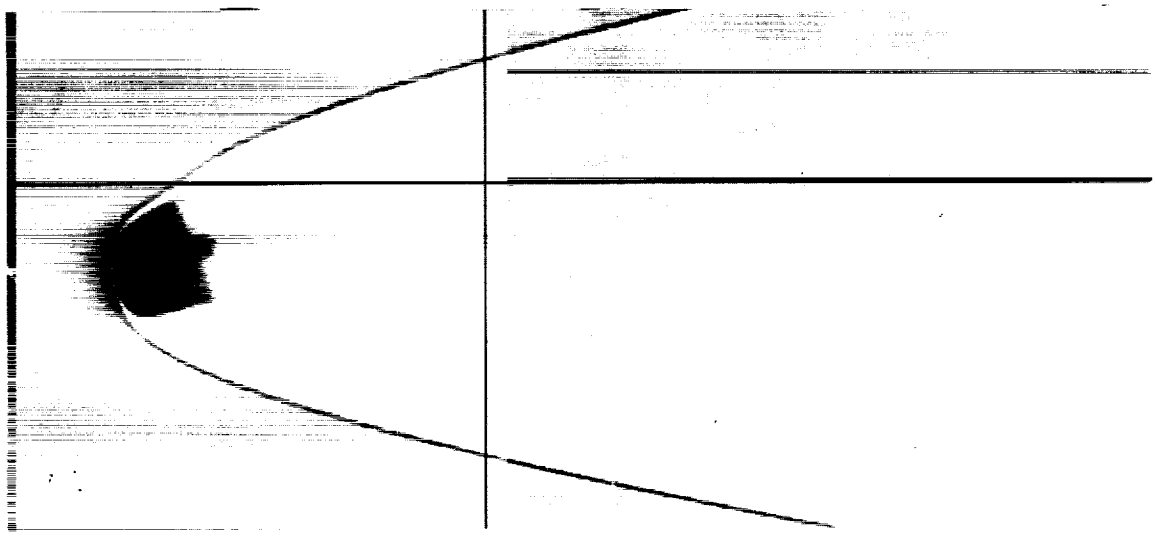

$\alpha = -22.94$

(d) $M = 8.5$, $Re = 0.2 \times 10^6$

Figure 3.- Concluded.

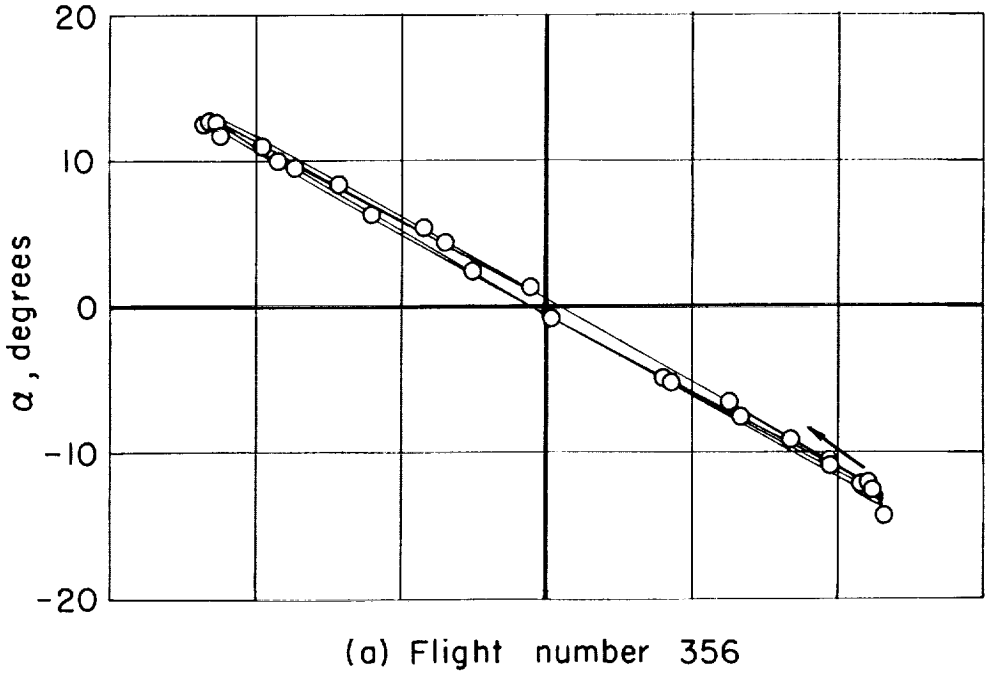

(a) Flight number 356

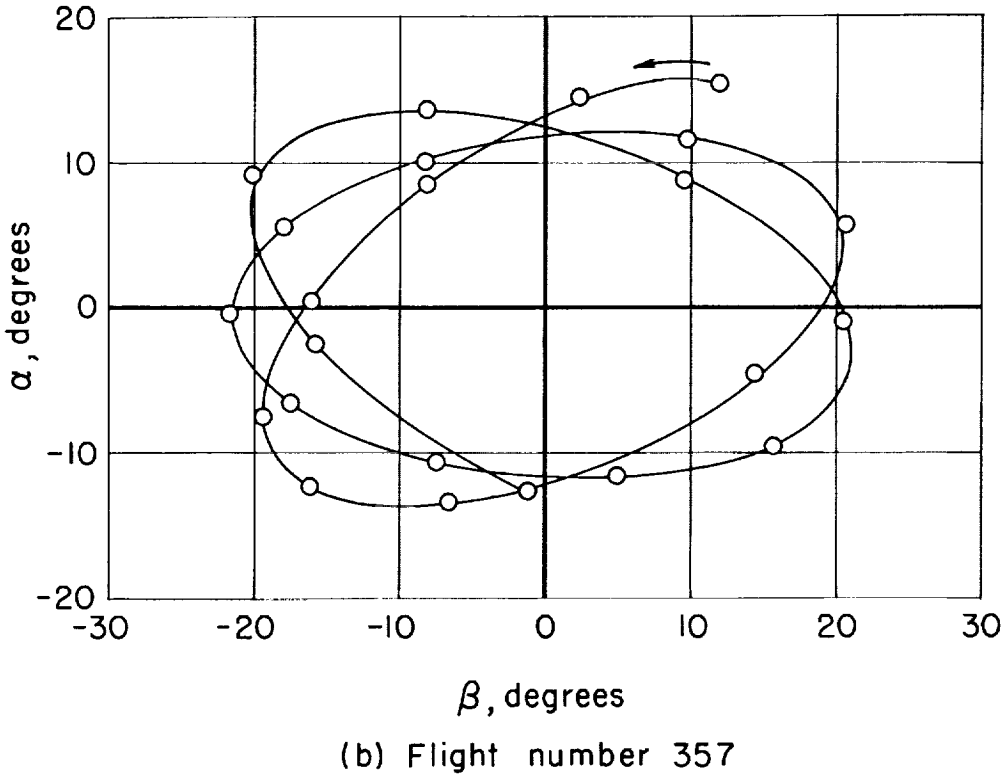

(b) Flight number 357

Figure 4.- Typical pitching and yawing motions.

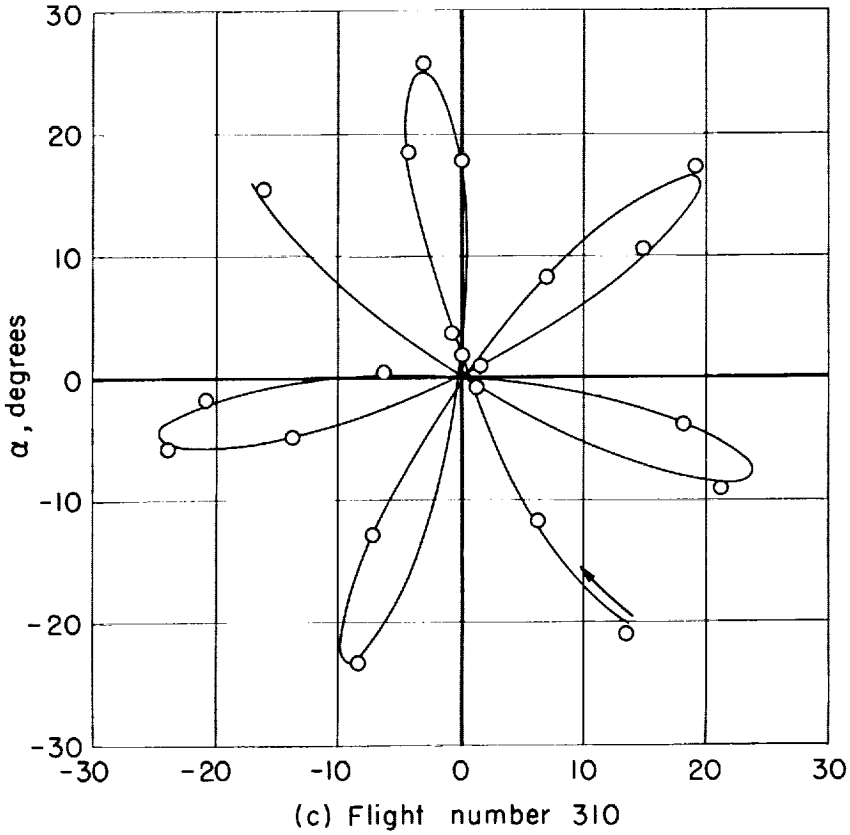

(c) Flight number 310

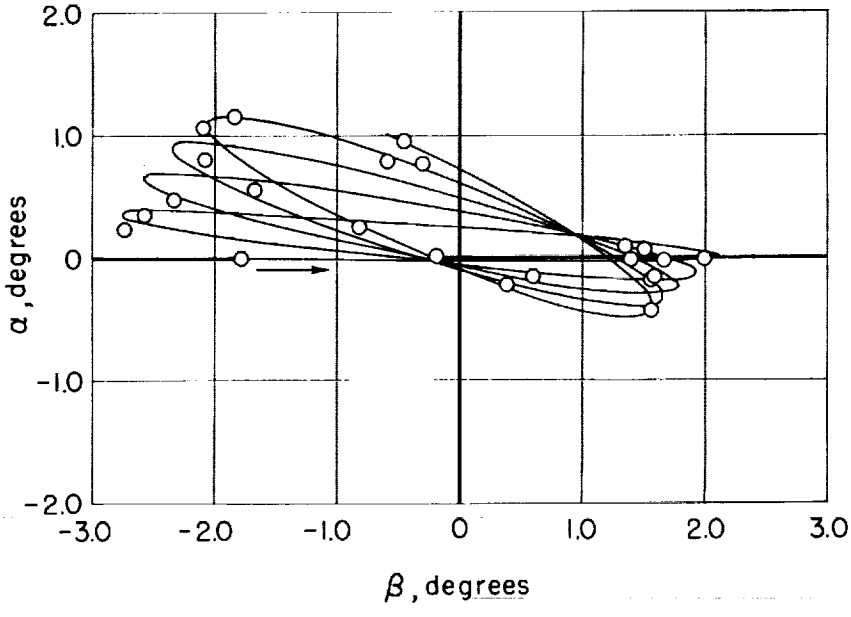

(d) Flight number 302

Figure 4.- Concluded.

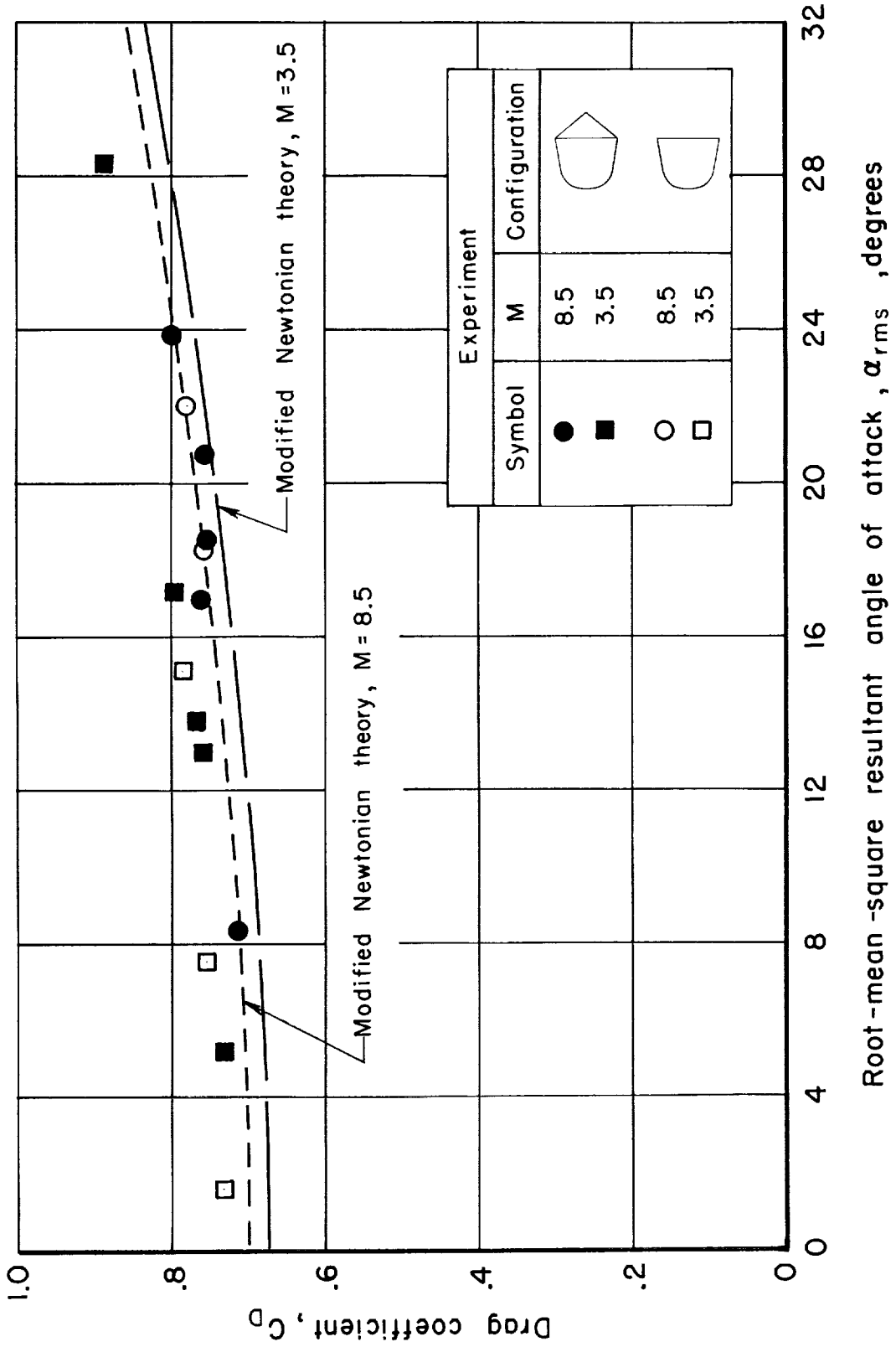

Figure 5.- Drag results.

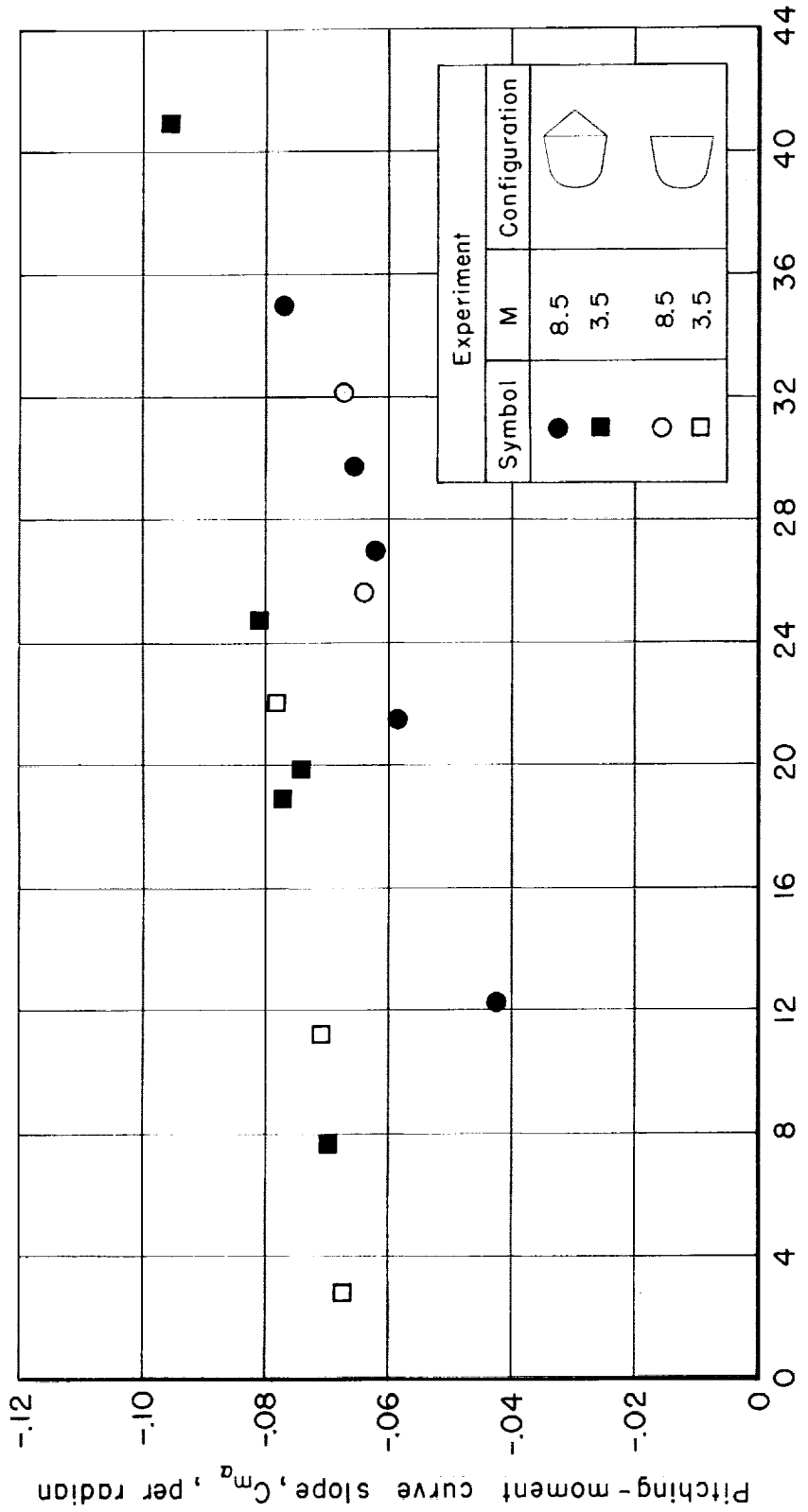

Figure 6.- Static stability results (linear analysis of data).

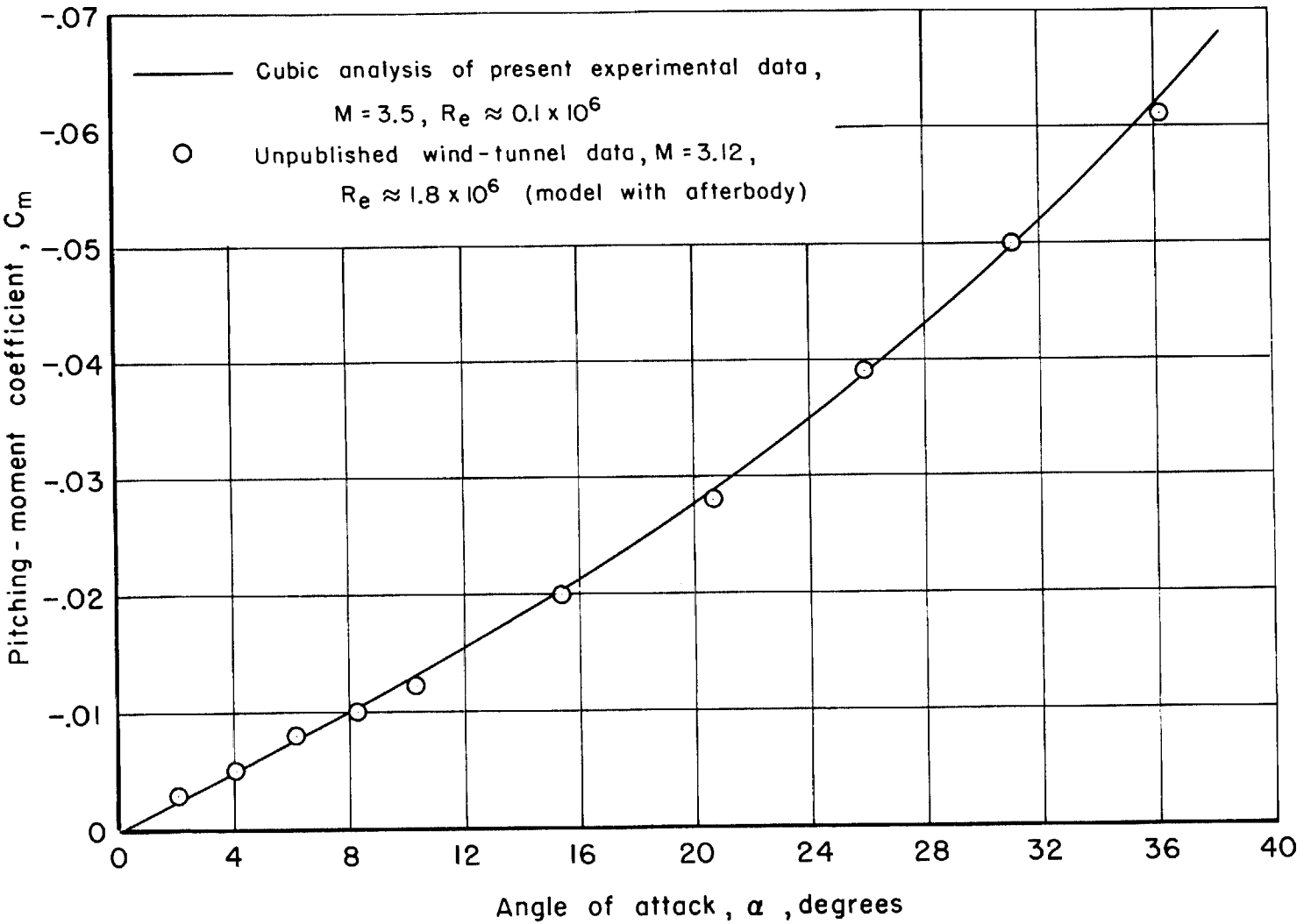

Figure 7.- Pitching-moment data obtained from present tests compared with unpublished wind-tunnel data; $x_{cg}/d = 0.482$.

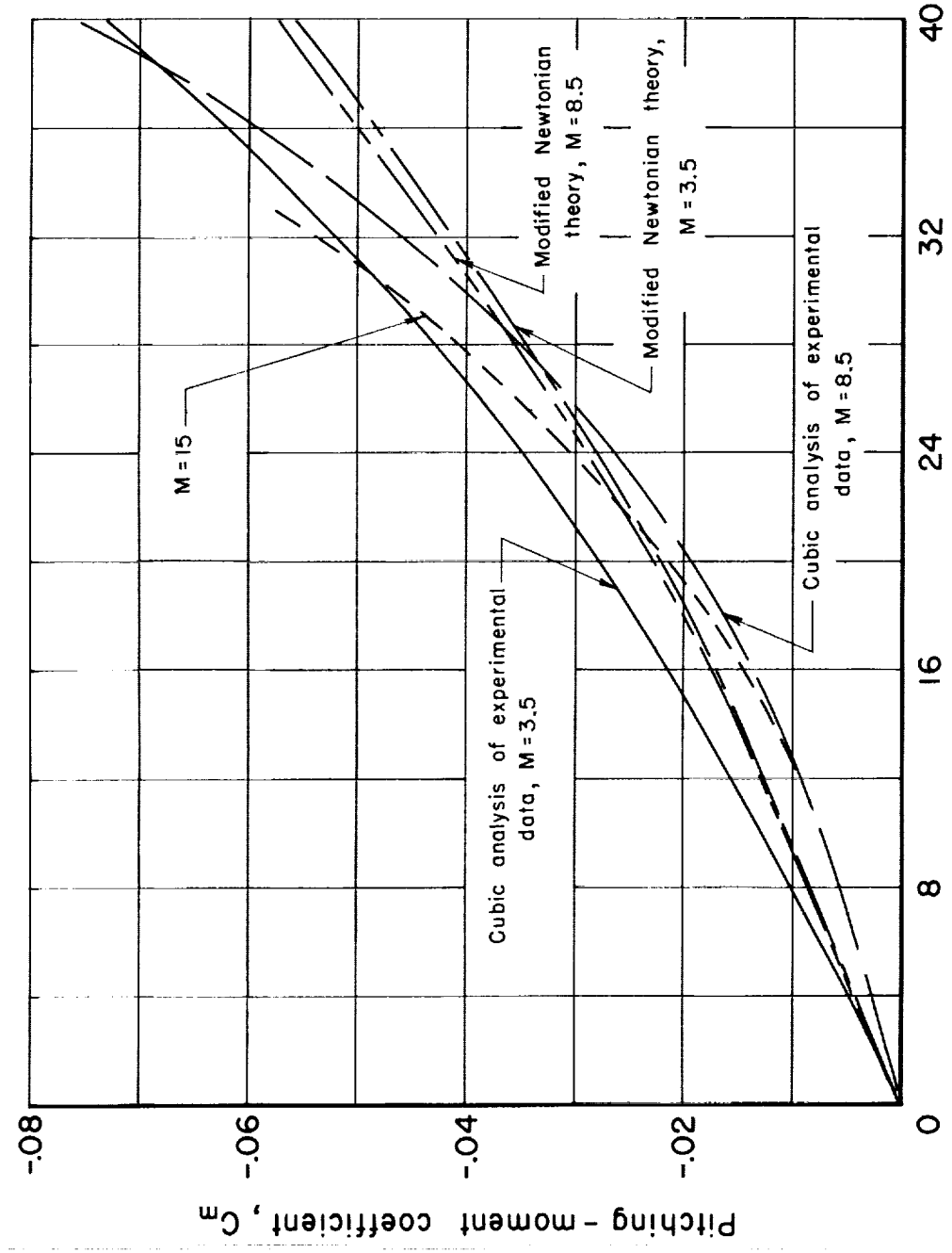

Figure 8.- Effect of Mach number on pitching moment for both configurations; $x_{cg}/d = 0.482$.

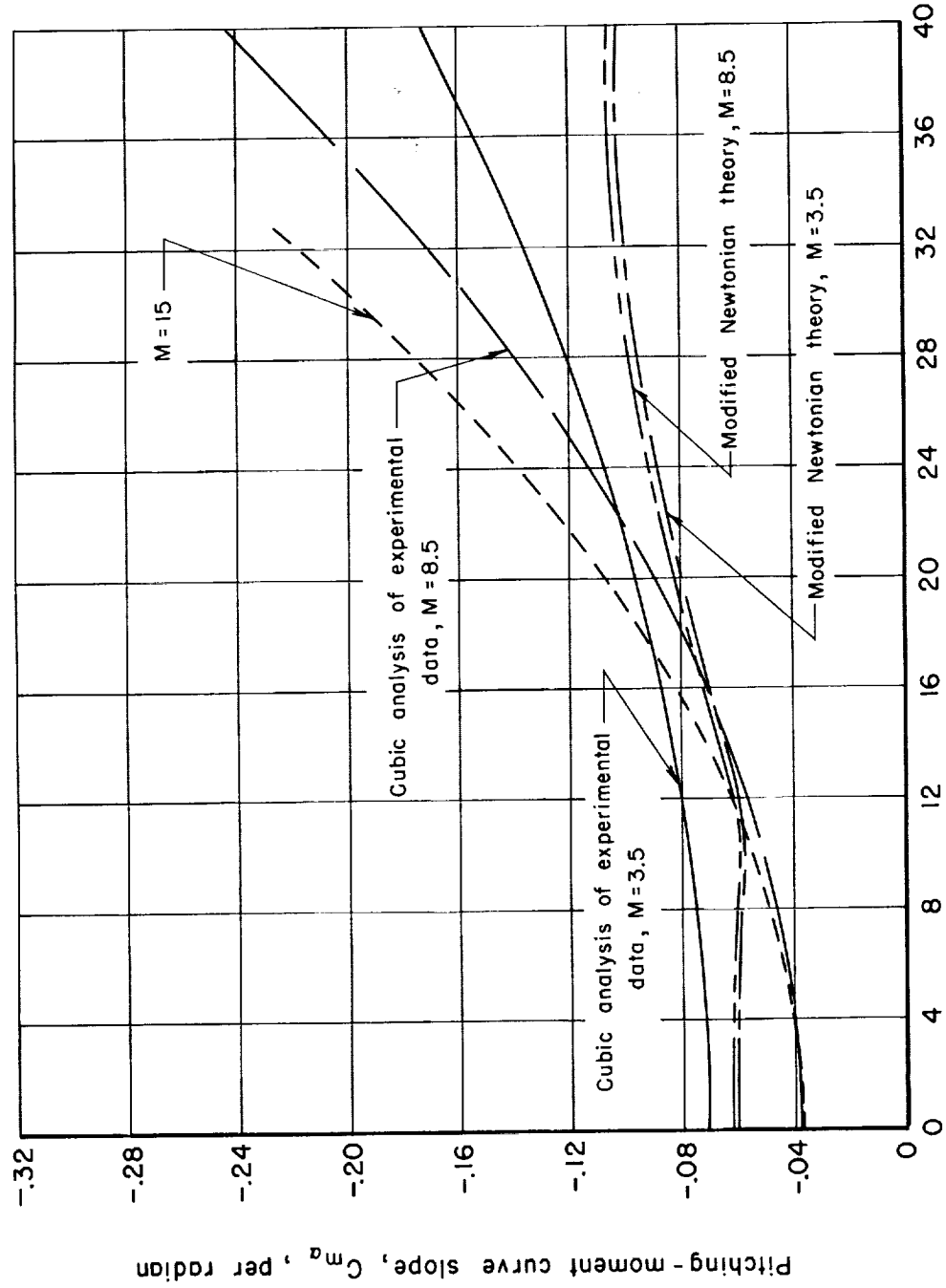

Figure 9.- Effect of Mach number on pitching-moment-curve slope for both configurations; $x_{cg}/d = 0.482$.

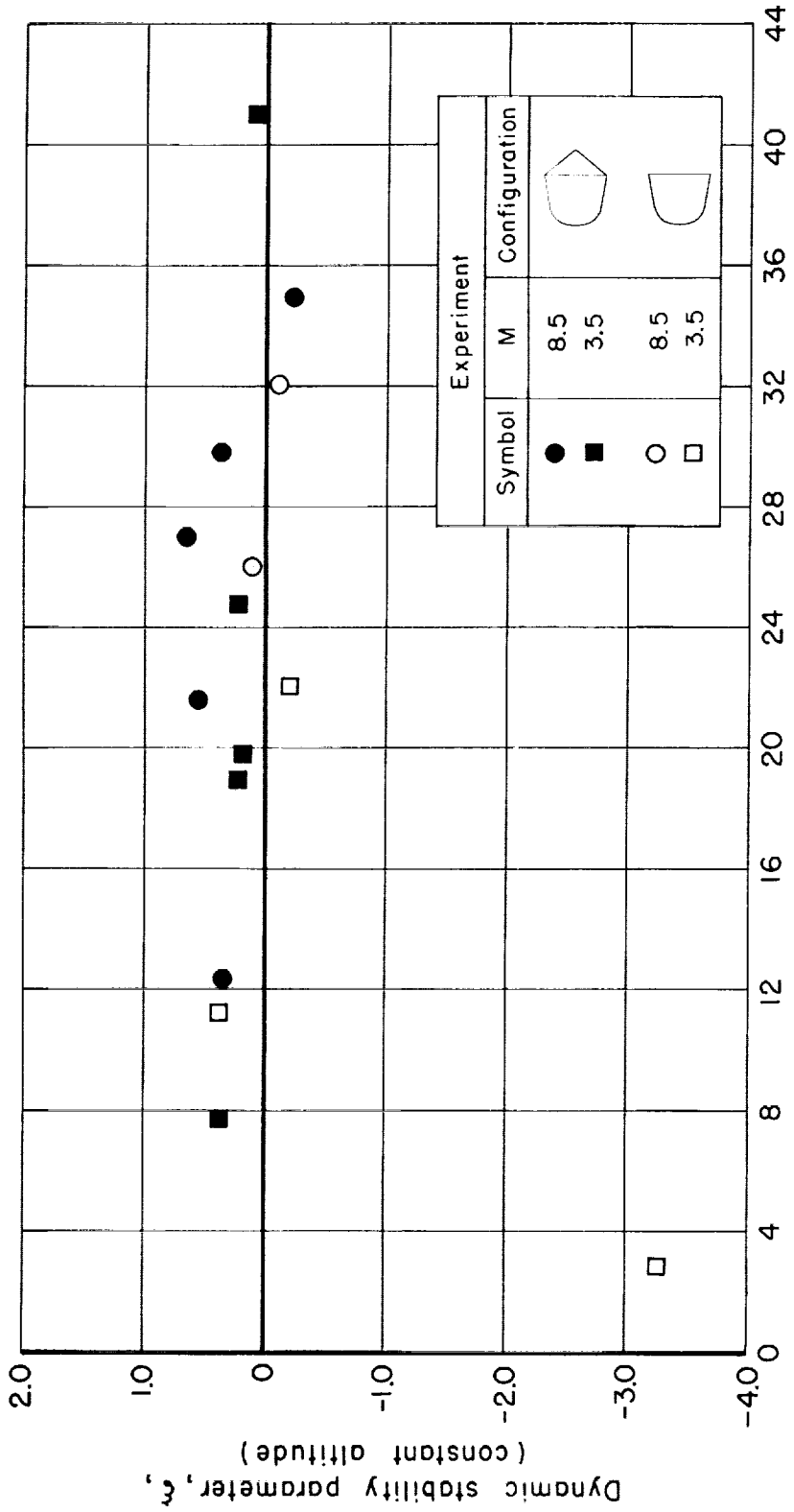

Figure 10.- Comparison of the dynamic stability parameter, ξ, for both configurations.

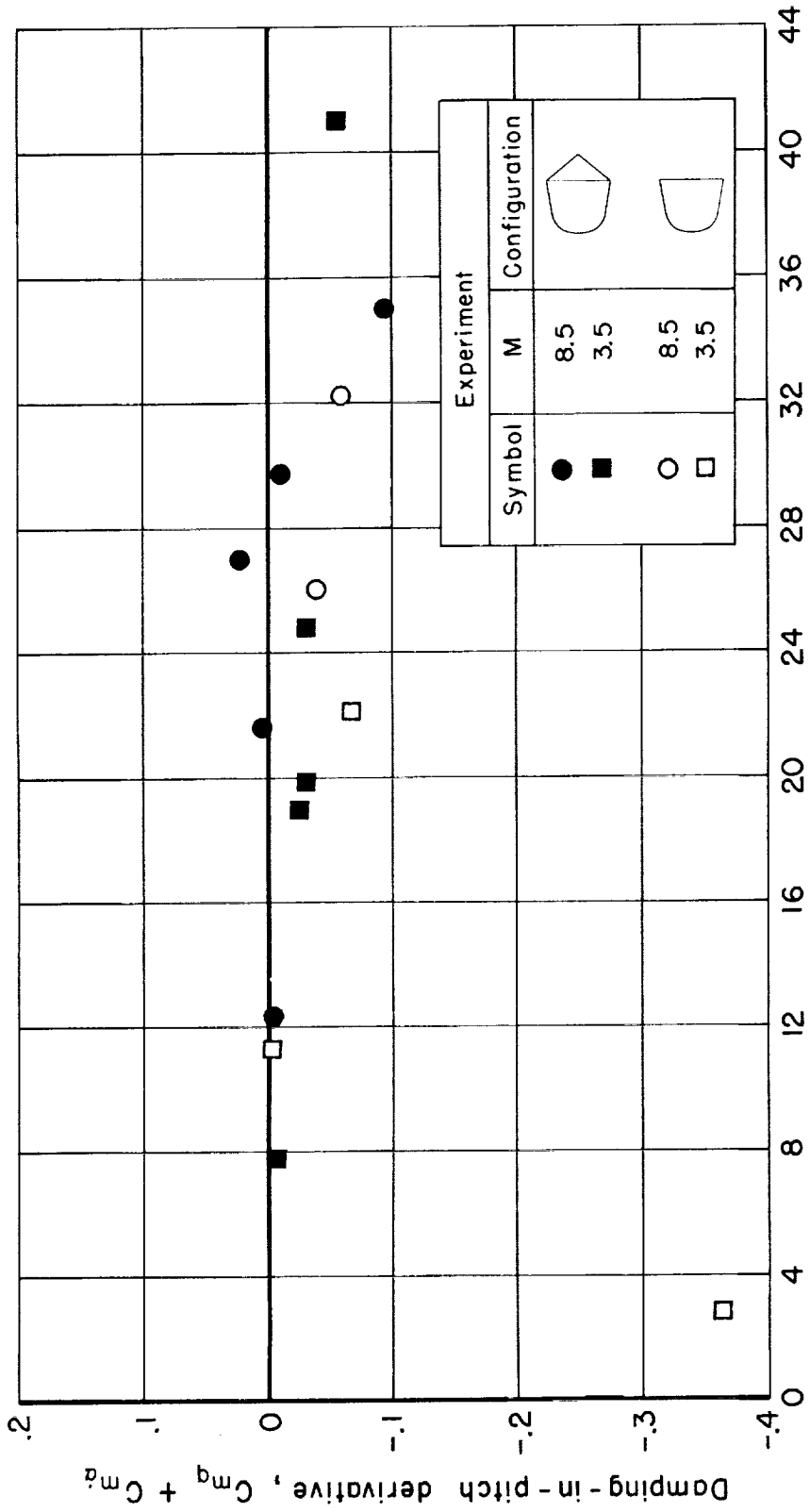

Figure 11.- Comparison of the damping-in-pitch derivative, $C_{m_q} + C_{m_{\dot{\alpha}}}$, for both configurations.

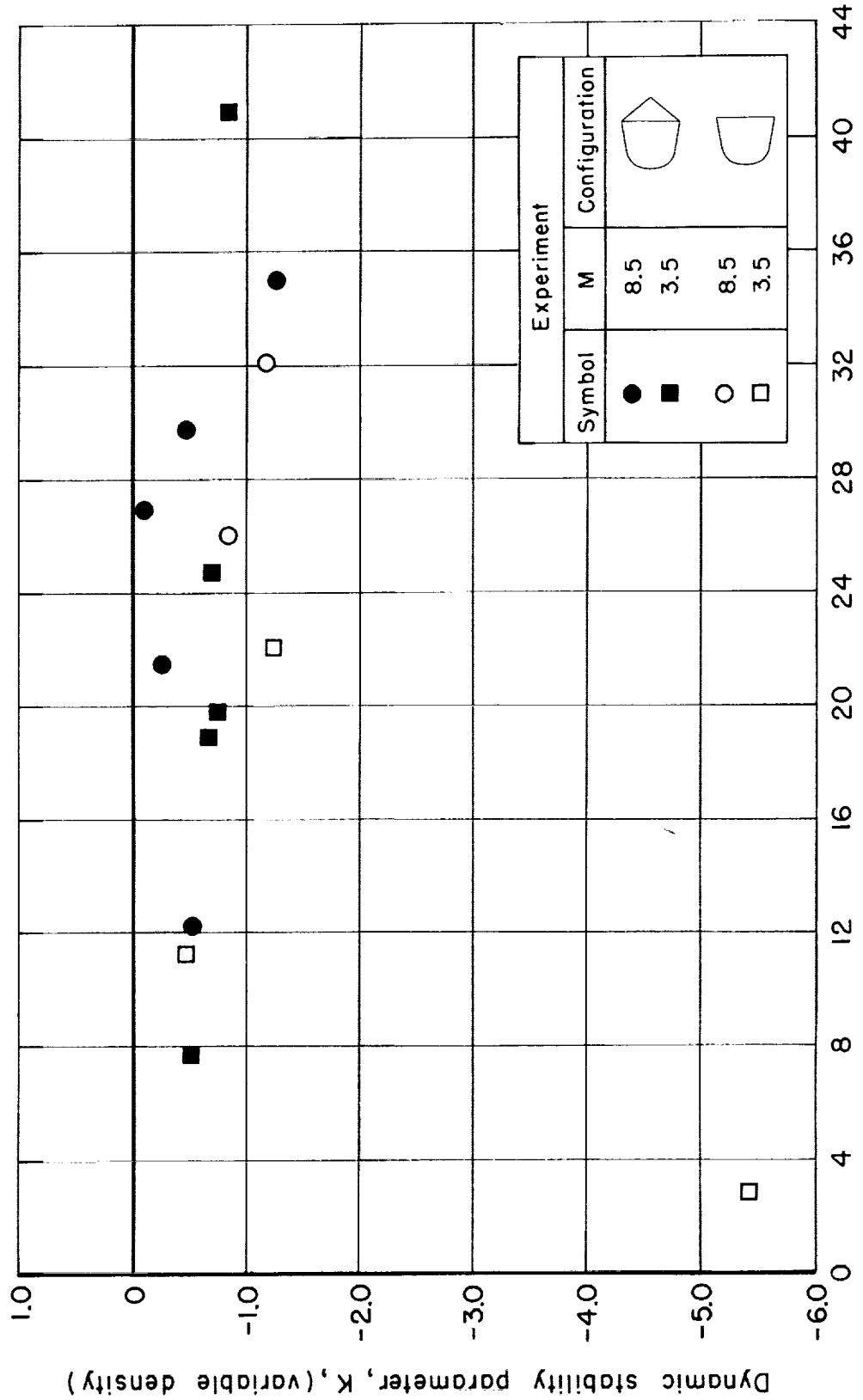

Figure 12.- Comparison of the dynamic stability parameter, K, for both configurations.

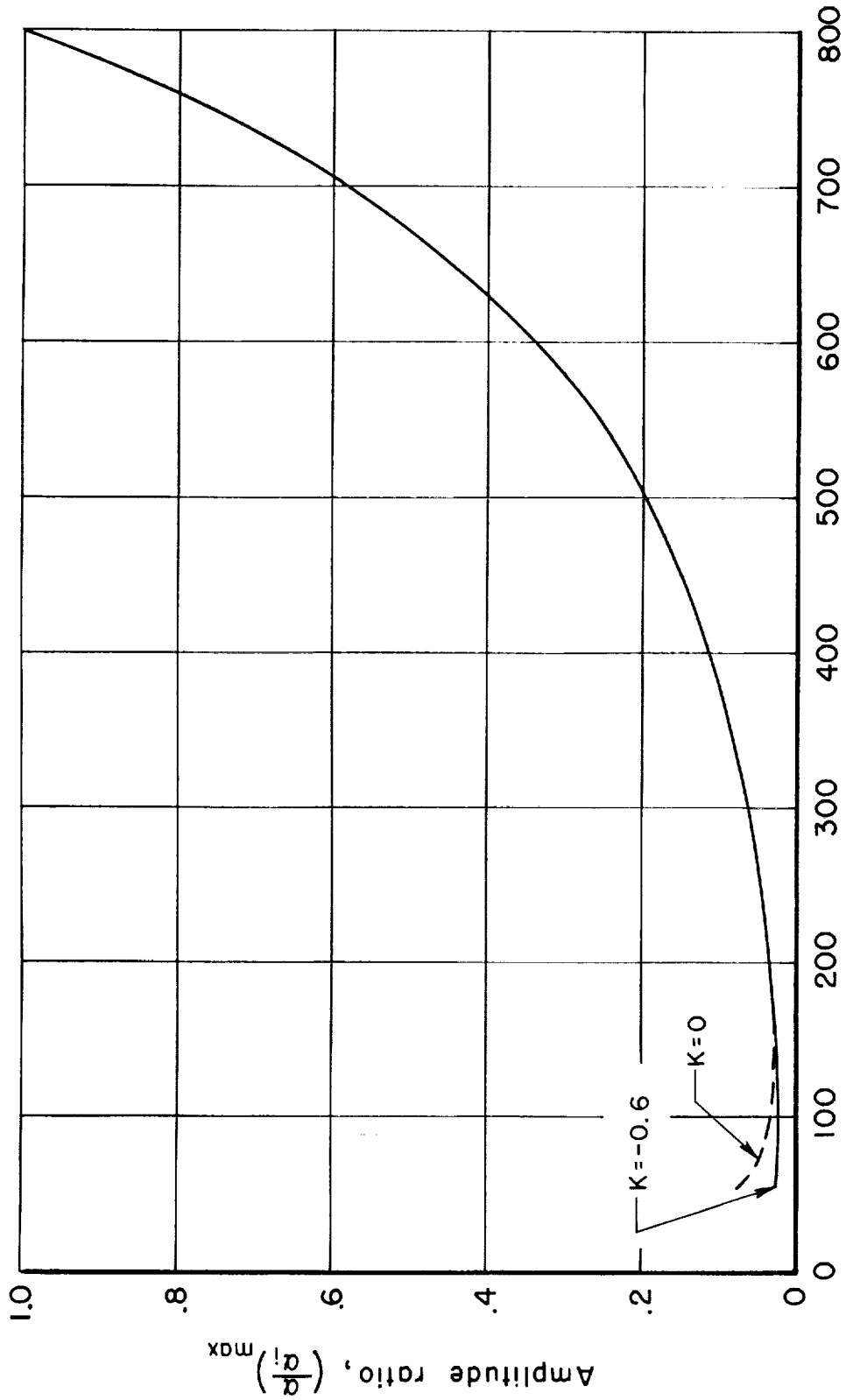

Figure 13.- Oscillation-amplitude histories of the configuration entering a model Martian atmosphere.

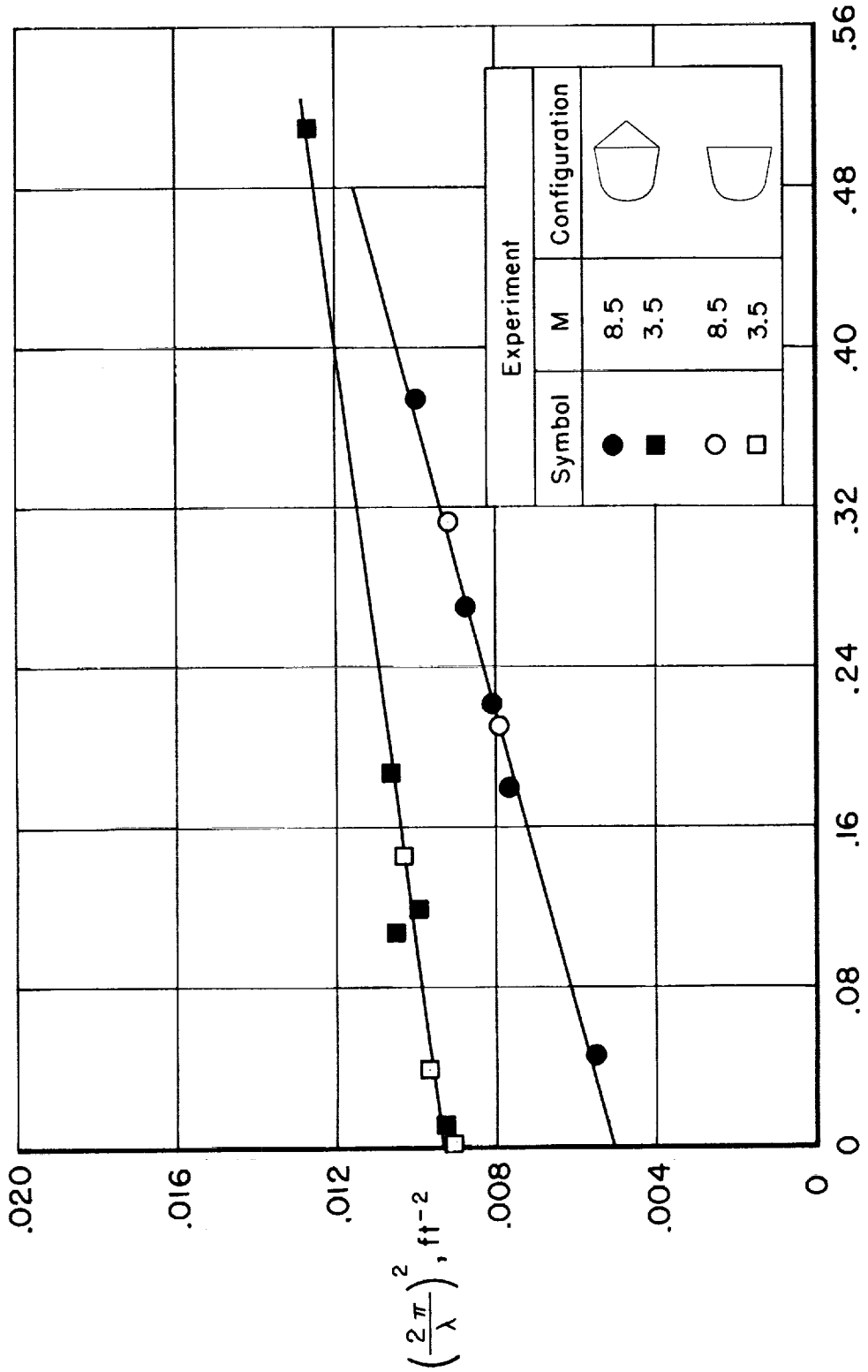

Figure 14.- Variations of the observed frequency with amplitudes of the motion.

NASA TN D-1299
National Aeronautics and Space Administration.
FREE-FLIGHT MEASUREMENTS OF THE STATIC AND DYNAMIC STABILITY AND DRAG OF A 10^{o} BLUNTED CONE AT MACH NUMBERS 3.5 AND 8.5.
Peter F. Intrieri. May 1962. 36p. OTS price, $1.00. (NASA TECHNICAL NOTE D-1299)

Static and dynamic stability and drag were measured in a pressurized ballistic range at nominal Mach numbers of 3.5 and 8.5 and at a nominal Reynolds number of 0.15×10^{6}. The experimental static-stability data were found to fit a cubic pitching-moment curve. The measured dynamic-stability results were used to calculate the oscillatory behavior of the configuration flying an example entry trajectory through a model of the Martian atmosphere.

Copies obtainable from NASA, Washington

I. Intrieri, Peter F.
II. NASA TN D-1299

(Initial NASA distribution:
2, Aerodynamics, missiles and space vehicles;
5, Atmospheric entry;
20, Fluid mechanics;
48, Space vehicles;
50, Stability and control.)

NASA

NASA TN D-1299
National Aeronautics and Space Administration.
FREE-FLIGHT MEASUREMENTS OF THE STATIC AND DYNAMIC STABILITY AND DRAG OF A 10^{o} BLUNTED CONE AT MACH NUMBERS 3.5 AND 8.5.
Peter F. Intrieri. May 1962. 36p. OTS price, $1.00. (NASA TECHNICAL NOTE D-1299)

Static and dynamic stability and drag were measured in a pressurized ballistic range at nominal Mach numbers of 3.5 and 8.5 and at a nominal Reynolds number of 0.15×10^{6}. The experimental static-stability data were found to fit a cubic pitching-moment curve. The measured dynamic-stability results were used to calculate the oscillatory behavior of the configuration flying an example entry trajectory through a model of the Martian atmosphere.

Copies obtainable from NASA, Washington

I. Intrieri, Peter F.
II. NASA TN D-1299

(Initial NASA distribution:
2, Aerodynamics, missiles and space vehicles;
5, Atmospheric entry;
20, Fluid mechanics;
48, Space vehicles;
50, Stability and control.)

NASA

NASA TN D-1299
National Aeronautics and Space Administration.
FREE-FLIGHT MEASUREMENTS OF THE STATIC AND DYNAMIC STABILITY AND DRAG OF A 10^{o} BLUNTED CONE AT MACH NUMBERS 3.5 AND 8.5.
Peter F. Intrieri. May 1962. 36p. OTS price, $1.00. (NASA TECHNICAL NOTE D-1299)

Static and dynamic stability and drag were measured in a pressurized ballistic range at nominal Mach numbers of 3.5 and 8.5 and at a nominal Reynolds number of 0.15×10^{6}. The experimental static-stability data were found to fit a cubic pitching-moment curve. The measured dynamic-stability results were used to calculate the oscillatory behavior of the configuration flying an example entry trajectory through a model of the Martian atmosphere.

Copies obtainable from NASA, Washington

I. Intrieri, Peter F.
II. NASA TN D-1299

(Initial NASA distribution:
2, Aerodynamics, missiles and space vehicles;
5, Atmospheric entry;
20, Fluid mechanics;
48, Space vehicles;
50, Stability and control.)

NASA

NASA TN D-1299
National Aeronautics and Space Administration.
FREE-FLIGHT MEASUREMENTS OF THE STATIC AND DYNAMIC STABILITY AND DRAG OF A 10^{o} BLUNTED CONE AT MACH NUMBERS 3.5 AND 8.5.
Peter F. Intrieri. May 1962. 36p. OTS price, $1.00. (NASA TECHNICAL NOTE D-1299)

Static and dynamic stability and drag were measured in a pressurized ballistic range at nominal Mach numbers of 3.5 and 8.5 and at a nominal Reynolds number of 0.15×10^{6}. The experimental static-stability data were found to fit a cubic pitching-moment curve. The measured dynamic-stability results were used to calculate the oscillatory behavior of the configuration flying an example entry trajectory through a model of the Martian atmosphere.

Copies obtainable from NASA, Washington

I. Intrieri, Peter F.
II. NASA TN D-1299

(Initial NASA distribution:
2, Aerodynamics, missiles and space vehicles;
5, Atmospheric entry;
20, Fluid mechanics;
48, Space vehicles;
50, Stability and control.)

NASA

NASA TN D-1299
National Aeronautics and Space Administration.
FREE-FLIGHT MEASUREMENTS OF THE STATIC AND DYNAMIC STABILITY AND DRAG OF A 10^{o} BLUNTED CONE AT MACH NUMBERS 3.5 AND 8.5.
Peter F. Intrieri. May 1962. 36p. OTS price, $1.00. (NASA TECHNICAL NOTE D-1299)

Static and dynamic stability and drag were measured in a pressurized ballistic range at nominal Mach numbers of 3.5 and 8.5 and at a nominal Reynolds number of 0.15×10^{6}. The experimental static-stability data were found to fit a cubic pitching-moment curve. The measured dynamic-stability results were used to calculate the oscillatory behavior of the configuration flying an example entry trajectory through a model of the Martian atmosphere.

Copies obtainable from NASA, Washington

I. Intrieri, Peter F.
II. NASA TN D-1299

(Initial NASA distribution:
2, Aerodynamics, missiles and space vehicles;
5, Atmospheric entry;
20, Fluid mechanics;
48, Space vehicles;
50, Stability and control.)

NASA

NASA TN D-1299
National Aeronautics and Space Administration.
FREE-FLIGHT MEASUREMENTS OF THE STATIC AND DYNAMIC STABILITY AND DRAG OF A 10^{o} BLUNTED CONE AT MACH NUMBERS 3.5 AND 8.5.
Peter F. Intrieri. May 1962. 36p. OTS price, $1.00. (NASA TECHNICAL NOTE D-1299)

Static and dynamic stability and drag were measured in a pressurized ballistic range at nominal Mach numbers of 3.5 and 8.5 and at a nominal Reynolds number of 0.15×10^{6}. The experimental static-stability data were found to fit a cubic pitching-moment curve. The measured dynamic-stability results were used to calculate the oscillatory behavior of the configuration flying an example entry trajectory through a model of the Martian atmosphere.

Copies obtainable from NASA, Washington

I. Intrieri, Peter F.
II. NASA TN D-1299

(Initial NASA distribution:
2, Aerodynamics, missiles and space vehicles;
5, Atmospheric entry;
20, Fluid mechanics;
48, Space vehicles;
50, Stability and control.)

NASA

NASA TN D-1299
National Aeronautics and Space Administration.
FREE-FLIGHT MEASUREMENTS OF THE STATIC AND DYNAMIC STABILITY AND DRAG OF A 10^{o} BLUNTED CONE AT MACH NUMBERS 3.5 AND 8.5.
Peter F. Intrieri. May 1962. 36p. OTS price, $1.00. (NASA TECHNICAL NOTE D-1299)

Static and dynamic stability and drag were measured in a pressurized ballistic range at nominal Mach numbers of 3.5 and 8.5 and at a nominal Reynolds number of 0.15×10^{6}. The experimental static-stability data were found to fit a cubic pitching-moment curve. The measured dynamic-stability results were used to calculate the oscillatory behavior of the configuration flying an example entry trajectory through a model of the Martian atmosphere.

Copies obtainable from NASA, Washington

I. Intrieri, Peter F.
II. NASA TN D-1299

(Initial NASA distribution:
2, Aerodynamics, missiles and space vehicles;
5, Atmospheric entry;
20, Fluid mechanics;
48, Space vehicles;
50, Stability and control.)

NASA

NASA TN D-1299
National Aeronautics and Space Administration.
FREE-FLIGHT MEASUREMENTS OF THE STATIC AND DYNAMIC STABILITY AND DRAG OF A 10^{o} BLUNTED CONE AT MACH NUMBERS 3.5 AND 8.5.
Peter F. Intrieri. May 1962. 36p. OTS price, $1.00. (NASA TECHNICAL NOTE D-1299)

Static and dynamic stability and drag were measured in a pressurized ballistic range at nominal Mach numbers of 3.5 and 8.5 and at a nominal Reynolds number of 0.15×10^{6}. The experimental static-stability data were found to fit a cubic pitching-moment curve. The measured dynamic-stability results were used to calculate the oscillatory behavior of the configuration flying an example entry trajectory through a model of the Martian atmosphere.

Copies obtainable from NASA, Washington

I. Intrieri, Peter F.
II. NASA TN D-1299

(Initial NASA distribution:
2, Aerodynamics, missiles and space vehicles;
5, Atmospheric entry;
20, Fluid mechanics;
48, Space vehicles;
50, Stability and control.)

NASA